Colloid/Contaminant Co–Transport in Porous Fractured Media

by

Tanya Bilezikjian

A dissertation submitted in partial satisfaction of the
requirements for the degree of
Master of Science

in

Engineering

in the

GRADUATE DIVISION
of the
UNIVERSITY of CALIFORNIA at IRVINE

Committee in charge:

Professor Constantinos V. Chrysikopoulos, Chair
Professor Brett F. Sanders
Professor Jan W. S. Scherfig

2001

Colloid/Contaminant Co–Transport in Porous Fractured Media

The dissertation of Tanya Bilezikjian is approved:

_____

Chair   Date

_____

                                                                           Date

_____

                                                                           Date

University of California at IRVINE

2001

To my family

Contents

Nomenclature

A_p	cross–sectional area of a sorbed colloid, L^2.
b	uniform fracture aperture, L.
$\overline{b}$	mean aperture of a variable aperture fracture, L.
$b(x, y)$	local fracture aperture, L.
$\mathcal{C}$	number of contaminants exiting a fracture.
$\mathcal{C}^*$	number of contaminants sorbed to fracture and matrix walls.
$\mathcal{C}_o$	total number of contaminants in a plume.
d_p	colloid particle diameter, L.
$\mathcal{D}$	molecular diffusion coefficient of a colloid or contaminant particle, L^2/t.
$\mathcal{D}_{\text{matrix}}$	molecular diffusion coefficient of a contaminant within the matrix, L^2/t.
D_{eff}	effective dispersion coefficient of a colloid plume, L^2/t.
D_{Taylor}	Taylor dispersion coefficient of a contaminant plume, L^2/t.
$f(z)$	Gaussian probability density function.
$F(n^*)$	dynamic blocking function.
g	gravitational acceleration, L/t^2.
$h(x, y)$	piezometric head, L.
i	element number of a variable aperture fracture in the x–direction.
j	element number of a variable aperture fracture in the y–direction.
k	Boltzmann's constant, ML^2/Tt^2.
K_n	cotransport sorption rate coefficient, L/t.
m	numerical step number in the particle tracking equation.
n_o	initial number concentration of colloid particles, $1/L^3$.
$\mathcal{N}$	number of colloids exiting a fracture.
$\mathcal{N}^*$	total number of sorbed colloids.
$\mathcal{N}_o$	total number of monodisperse particles in a plume.
p	probability of colloid attachment per wall encounter.
P	local fluid pressure, M/Lt^2.
$P_{\text{cont}}(\Delta t)$	probability of contaminant wall sorption per time step.
$P(z)$	probability of a colloid entering the fracture at location z.
$Rn(0, 1)$	uniformly distributed random number between 0 and 1.
t	time, t.
Δt	time step for a particle tracking algorithm, t.
T	absolute temperature of the interstitial fluid, T.
u_x	local Poiseuille fluid velocity in the x–direction, L/t.
$\overline{u}_x$	mean fluid velocity in the x–direction, L/t.
u_y	local fluid velocity in the y–direction for a variable aperture fracture, L/t.

$\overline{u}_y$ mean fluid velocity in the y–direction for a variable aperture fracture, L/t.

u_z local fluid velocity in the z–direction, L/t.

$U_{\mathcal{D}}$ deterministic velocity due to a diffusivity gradient, L/t.

U_{eff} effective velocity of a contaminant plume, L/t.

$U_{\max}$ maximum, or centerline, velocity in a fracture, L/t.

U_θ deterministic velocity due to a porosity gradient, L/t.

x coordinate along the fracture length, L.

y coordinate along the fracture width, L.

z coordinate normal to the fracture surface, L.

z_{matrix} contaminant's z–location when diffusing within matrix, L.

Z a standard normally distributed random number.

Subscripts

eff   effective parameter.

d distribution.

DBF   dynamic blocking function.

i index indicating the element in the y–direction.

j index indicating the element in the x–direction.

matrix   indicates that contaminant has diffused into surrounding matrix.

max   maximum value.

p particle.

Taylor   indicates the Taylor dispersion coefficient

Greek Letters

β parameter defining hydrodynamic shadow effect for colloids sorbed to fracture wall.

γ fluid specific weight, M/L^2t^2.

$\epsilon(t,x,y)$ coefficient of surface coverage by colloids, equal to $A_p n^*(t,x,y)$.

$\epsilon_{\max}$ maximum coefficient of surface coverage by colloids.

θ matrix porosity.

κ multiplication constant.

μ fluid dynamic viscosity, M/Lt.

μ_d mean of the Gaussian distribution, equal to 0.

ρ fluid density, M/L^3.

ϕ repulsive interaction energy between a particle and the fracture surface, ML^2/t^3.

σ standard deviation.

$\sigma^2_{\ln b}$ variance of log aperture.

ξ correlation length of the fracture aperture fluctuations, L.

τ log–travel time, equal to $\ln \Sigma \Delta t$.

$\Omega(z)$ probability density function of particle z–loctions after one time step.

List of Figures

List of Tables

Acknowledgements

My deepest thanks go to my family, whose consistent love, support, advice and encouragement inspired me to pursue my education. To my father, Zaven Bilezikjian, whom I respect and admire; to Sandra and Mark, my brother and sister as well as my best friends, both of whom I am so proud of; to Ashleigh Aitken, after twenty two years of friendship you have become my sister in my heart, and also my best friend; to my aunts Berta and Louise who have set an example of the type of woman I aspire to become; to my uncle Vahe, who helped me with my math homework; to my uncle Richard, always ready to laugh; to my beautiful and loving grandmothers, Nanny and Mimi, who always told me I could achieve anything I wanted... Nanny, I think about you and miss you every day; to my loving and supportive mother, Sherry Stewart; and finally to my blue-eyed Papa – I know you are looking down on me from heaven and smiling. You have all believed in me and each of you has enriched my life beyond the ability of words to describe.

I owe sincere appreciation to my advisor, Dr. Constantinos Chrysikopoulos, first for extending to me the honor of an invitation to attend graduate school, and also for the knowledge and confidence he has imparted to me. To Dr. Scott James, my surrogate advisor, office mate and steadfast friend, you have been a constant source of information, advice and guidance. I couldn't have done this without you. To Dr. Brett Sanders, I thank you for the generosity you have shown me with your time, your advice, (and your computers!). Working as your teaching assistant was

one of my most rewarding and enriching experiences as a graduate student. And to Dr. Jan Scherfig, your support and assistance were greatly appreciated. I would like to acknowledge several professors whose courses I had the pleasure of taking: Dr. Taagapera, Dr. Brant, Dr. Lankford, Dr. George, Dr. DaSilva, Dr. Sanders, Dr. James, and my advisor Dr. Chrysikopoulos. Each of these gifted instructors enhanced my education beyond the information they imparted in class by fueling my desire to gain knowledge and understand the world around me, and each of them is a credit to U.C. Irvine.

To my friend Carrie Green, we made lasting memories, had good times, suffered through and excelled in classes, cried on each other's shoulders and ultimately built a friendship that I will always treasure. To Ashleigh Aitken, your strength, generosity, loyalty and love have taught me the meaning of friendship. I am honored to have you in my life. To Amber Waltman, my kindred spirit in the school of engineering; to Suzanne Brown, here's to the Pacific Coast Triathlon; and to Mike Papac, Jorge Luna and Bruce McCarthy, each of you owns a permanent part of my heart. To my current and former office mates, Eric Vogler, Matt Bao, Allyson Chu, David Jaffe and Carrie Green; thank you for the camraderie and friendship we all shared.

Finally, I wish to extend my thanks to the staff of the Civil and Environmental Engineering office, and particularly to John Sommerhauser. You work behind the scenes but your dedication and energy are greatly appreciated.

Abstract

Colloid/Contaminant Co–Transport in Porous Fractured Media

by

Tanya Bilezikjian

Master of Science in Engineering

University of California at IRVINE

Professor Constantinos V. Chrysikopoulos, Chair

A three–dimensional particle tracking model is developed to characterize the long term spatial and temporal effects of advection, molecular diffusion, Taylor dispersion, fracture wall deposition, matrix diffusion, and co–transport on two discrete plumes (monodisperse colloids and aqueous phase contaminants) flowing through a spatially variable aperture fracture. Contaminant particles travel by advection and diffusion and may sorb onto both fracture walls and colloid particles, as well as diffuse into and sorb onto the surrounding porous rock matrix. Colloid particles also travel by advection and diffusion and may sorb onto fracture walls, but do not penetrate the rock matrix. A linear dynamic blocking function is used to govern attachment of colloid and contaminant particles onto fracture walls; and an irreversible kinetic isotherm is employed to describe contaminant sorption onto colloids. Ensemble averaged break-

through curves of many fracture realizations are used to compare arrival times of colloid and contaminant plumes at the fracture outlet. Results show that the presence of colloid particles enhances contaminant transport while matrix diffusion and sorption onto fracture walls retard the transport of contaminants.

0.1   Introduction

Colloid facilitated contaminant transport, or co–transport, will be a topic of concern and the subject of considerable research efforts while radioactive waste is stored in repositories located in either the saturated or unsaturated subsurface. Non–radioactive, but still toxic and carcinogenic, non–aqueous phase liquids (NAPLs), both dense (DNAPLs) and light (LNAPLs), and more readily soluble contaminants such as MTBE, may also be subject to co–transport phenomena. Leaking underground storage tanks, pipe fittings and waste containers, accidental spills, and illegal dumping activities provide pathways for these contaminants to enter the geosphere. Although low permeability rock media and salt formations are good candidates for waste sequestration sites, the presence of fractures and colloids in a saturated environment may provide an avenue and a means for enhanced transport of escaped radionuclides and other low solubility contaminants. Studies have revealed radionuclides much further afield than often expected, and attributed this to co–transport effects [*Ibaraki and Sudicky*, 1995] (more references).

Both high and low level radioactive waste burial or storage sites are often situated in low permeability bedrock, clay, granite, or salt deposits where diffusion is the primary transport mechanism available to aqueous particles. When waste storage containers leak, pools of very low solubility radioactive or toxic contaminants form that slowly dissolve into the interstitial fluid. Contaminant pools originating from urban sources such as underground gasoline storage tanks may behave similarly; however,

these pools are often located in fresh water aquifers, further emphasizing the need for accurate characterization of contaminant movement. These contaminant pools may remain in place for centuries, depending upon the extent of leakage, aqueous contaminant solubility, and sorption or reaction properties.

Characterizing the fate of colloids and reactive contaminants in fractured subsurface formations to better understand contemporary groundwater pollution problems is the focus of many recent studies [e.g. *Abdel-Salam and Chrysikopoulos*, 1995a, b; *Ibaraki and Sudicky*, 1995; *Kessler and Hunt*, 1994; *Johnson et al.*, 1996; *Chrysikopoulos and Abdel-Salam*, 1997] (reorder). These studies suggest that knowledge of the coupled hydrodynamic flow, contaminant transport, and surface reaction processes occuring in a single fracture is fundamental to improving our understanding of reactive contaminant transport in fractured media. Further, recent experimental and field studies indicate that contaminants can migrate while sorbed on the surface of colloid particles (add references). Consequently, colloids may affect the mobility of soluble contaminants in fractures as the sorbed contaminants assume the transport characteristics of the colloids that may be significantly different from their own. Factors that may have an impact on the extent of co–transport phenomena include individual particle surface charge, relative size of the particles, the pH or ionic strength of the water in the fracture, and van der Waals forces.

Colloids are present in the subsurface in the form of metal oxides, humic macromolecules, bacteria, and viruses [*Chrysikopoulos and Sim*, 1996]. In fractured media,

colloids are often formed by microerosion of minerals present in the solid matrix as a result of formation crushing in association with tectonic activity [*Drever*, 1985]. Colloid particles themselves may be contaminants, such as bacteria or viruses, or may become contaminants after a sorption reaction with contaminant particles, like radionuclides. Because colloids have a high surface area per unit mass, they provide contaminant particles with the opportunity to transport while sorbed onto their surface [*McCarthy and Zachara*, 1989] (another reference). The omnipresence of colloids in the subsurface and their characteristic large surface areas have inspired extensive research in the area of co–transport of discrete plumes.

Aqueous contaminant particles, with diameters ranging from molecular to colloidal, are carried away from their source with the prevailing groundwater velocity, and plumes spread under the combined effects of advection and diffusion in porous media. Groundwater velocities in rock media are typically low, leaving molecular diffusion the primary contaminant driving force. Low porosity media often serve to retard particle transport as the advective travel distance such media is negligible. However, if a particle plume enters a water saturated fracture/fracture network within the porous bedrock, the local advective velocity typically increases by orders of magnitude, thereby enhancing particle transport. Thus, fractures provide preferential pathways for colloid and contaminant migration within the low permeability porous media.

Often contaminants have a high sorption affinity for the surrounding porous ma-

trix, resulting in significantly decreased contaminant concentrations short distances from the source. However, detection of contaminants far beyond expected travel distances suggests that an alternate transport mechanism exists. Colloids, ubiquitous in groundwater [*McCarthy and Degueldre*, 1993], are often considered a mobile third phase [*McCarthy and Zachara*, 1989]. Because colloids are present in groundwater, and because contaminant species often have a strong affinity for colloid particles, co–transport is the likely mechanism responsible for the observed enhanced transport of a contaminant plume.

The co–transport model assumes that complexed colloid and contaminant particles will travel according to the transport characteristics of the larger colloid particles. Therefore, a contaminant that has sorbed onto a colloid does not affect the colloid particle's transport due to the large difference in the size of the particles. This assumption, based on observations of enhanced contaminant transport in field studies, laboratory experiments and numerical modeling, has several explanations. First, colloids may travel at a velocity greater than the mean fluid velocity because they are excluded from the slowest moving portion of the flow (nearest the fracture walls) due to their finite size [*Small*, 1974]. Secondly, because of their low diffusivity and such factors as lift forces and possible electrostatic repulsion, colloids tend to remain in the center of the fracture and therefore are less likely to encounter a fracture wall, thereby reducing sorption probability [*McTigue et al.*, 1986]. Further, a contaminant that has sorbed onto a colloid may no longer sorb onto the fracture walls unless the

colloid to which it is attached does so, nor may it diffuse into the surrounding porous matrix due to the colloids' inability to enter small matrix pores, yielding a greater percentage of contaminants remaining within the fracture. Clearly, if co–transport mechanisms are not considered when modeling contaminant transport, the extent of contaminant migration may be grievously underestimated [*Grindrod*, 1993; *McCarthy and Degueldre*, 1993].

This research is based on a novel particle tracking algorithm that may be used to simulate laboratory or field situations through application of case–specific model parameters and evaluation of resulting breakthrough curves. Colloids and contaminants are tracked through many realizations of stochastically generated, three–dimensional, variable aperture fractues. The fracture models all have a constant specified mean, variance, and correlation length of fracture aperture fluctuations, with random seeds making each realization unique. Individual elution times for each colloid and contaminant particle from each fracture realization are incorporated into cumulative normalized ensemble average breakthrough curves. By comparing the shape of these curves, the individual and combined effects of various transport mechanisms and model parameters on particle transport behavior may be investigated.

To verify the accuracy of the particle tracking model, breakthrough curves for each plume are first compared with an analytical solution for a uniform aperture fracture, yielding excellent agreement. The first case presented shows results from a simplified simulation of two non–reacting plumes, colloids and contaminants, moving through

a uniform aperture fracture subject to advective and diffusive mass transfer. This model provides a base case, or reference for comparison as well as an opportunity to observe, unhindered by other processes, the individual effects of Taylor dispersion on each plume before implementing more complicated models. Next, model results of non–reacting colloid and contaminant plumes moving through a variable aperture fracture are presented and compared with the results from the uniform aperture fracture. Sorption and desorption reactions of colloids and contaminants with the fracture walls are considered, subject to a linear dynamic blocking function (DBF). The DBF accounts for the presence of previously deposited particles and serves to restrict further particle deposition as complete monolayer coverage of the fracture walls is approached. Cumulative normalized breakthrough curves for a range of contaminant wall sorption parameters, resulting in retardation of plume transport, are compared to the case of no fracture wall deposition. Next, matrix diffusion of contaminants is examined, with results again compared to the model simulation with no diffusion into the surrounding medium. Also, once a contaminant diffuses into the porous matrix it may sorb onto the walls of the matrix. Fracture wall deposition and matrix diffusion, the two retarding processes affecting the contaminant plume are then implemented simultaneously. This model manifestation, incorporating all of the transport mechanisms discussed so far is used for comparison with a co–transport case.

Each of the previously described simulations has superimposed additional trans-

port or retardation processes so that the model approaches an increasingly accurate simulation of a natural system. These preliminart model results have been developed so the effect of co–transport mechanisms may be observed in relation to each transport or retardation process affecting the plumes. Snapshots in time of the locations of contaminants as well as breakthrough curves are used to illustrate the effects of co–transport. Initially, the effect of variation of only the co–transport parameter (governing the affinity of the colloid and contaminant particles) within a variable aperture fracture is considered by comparison with the transport characteristics of a colloid plume and a non–reacting contaminant plume. Ultimately, the model incorporates the processes of matrix diffusion, wall sorption and desorption, and reversible particle–particle reaction to examine their combined effect on colloid and contaminant co–transport.

0.2 Numerical Formulation

0.2.1 Fracture Generation

Figure 0.1 is a simplified illustration of the general system modeled in this work; the quasi–three–dimensional fracture used in this study is 8 m long (x–direction) and 4 m wide (y–direction). The fracture plane is partitioned into 12,800 discrete square elements such that each 5×5 cm element exhibits a distinct aperture as illustrated in Figure 0.2. The aperture field in the fracture is generated stochastically
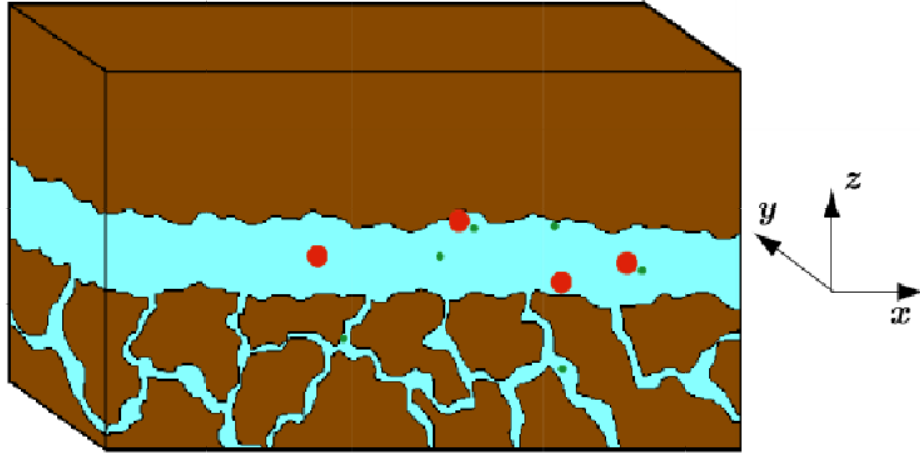
Figure 0.1: Schematic illustration of a quasi–three–dimensional fracture with spatially variable aperture, $b(x, y)$. Two migrating plumes (finitely sized colloid particles and molecular or point contaminant particles) are shown undergoing surface sorption, wall deposition, matrix diffusion and co–transport. Note that $z = 0$ m at the center of the fracture.

by the geostatistical code SPRT2D [*Gutjahr*, 1989]. It is assumed that the aperture

distribution in the fracture plane follows a log–normal distribution [*Johns et al.*, 1993;

Reimus et al., 1993; *Keller*, 1998] with preselected mean and variance. Furthermore,

the aperture distribution was assumed to vary spatially according to an isotropic

exponential autocovariance function with specified correlation length. In this work,

the average aperture of each fracture is $\bar{b} = 5 \times 10^{-5}$ m, the variance of the log aperture

is $\sigma_{\ln b}^2 = 0.015$, and the isotropic correlation length is $\xi = 1$ m. By definition, a

correlation length implies that for distances along the fracture plane smaller than

the correlation length the aperture values are likely to be similar, but at distances

greater than the correlation length there is no relation between apertures. Unique
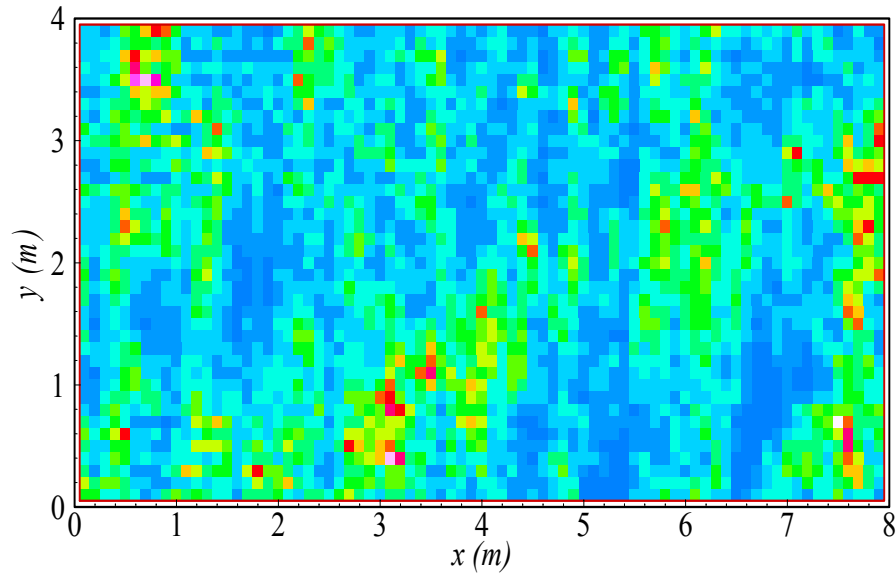
Figure 0.2: A realization of the aperture spatial distribution in the fracture plane. The fracture is partitioned into 160×80 equally sized elements. The gray scale illustrates apertures between 0.01 and 0.15 mm (here $0 \leq x \leq 8.0$ m, $0 \leq y \leq 4.0$ m, $\bar{b} = 5 \times 10^{-5}$ m, $\sigma_{\ln b}^2 = 0.15$, and $\xi = 1$ m).

realizations of the aperture field are obtained by changing the seed number of the random field generator.

A large number of fractures as well as a large number of particles per plume is used so that random noise, everpresent in stochastic simulations, is smoothed out through the averaging process. The same set of one hundred unique fracture realizations is used for each variation of model parameters. Ensemble averages of the resulting colloid and contaminant elution times are used to generate the cumulative normalized number breakthrough curves.

0.2.2 Calculation of Flow Field

The two–dimensional, steady–state partial differential equation describing flow within a spatially variable aperture fracture is [*Chrysikopoulos and Abdel-Salam*, 1997; *James*, 2001]

$$\frac{\partial}{\partial x}\left[b^3\left(x,y\right)\frac{\partial h\left(x,y\right)}{\partial x}\right] + \frac{\partial}{\partial y}\left[b^3\left(x,y\right)\frac{\partial h\left(x,y\right)}{\partial y}\right] = 0, \tag{0.1}$$

where $b(x,y)$ is the local fracture aperture and $h(x,y)$ is the piezometric head. Equation (0.1) is a stochastic partial differential equation because one of its parameters, namely $b(x,y)$, is a stochastic variable.

For each realization of the aperture field, the following five–point central finite difference numerical approximation is employed for the solution of the governing flow equation [*Hoffman*, 1992]

$$b^3_{i,j+1/2}h_{i,j+1} + b^3_{i,j-1/2}h_{i,j-1} + b^3_{i+1/2,j}h_{i+1,j} + b^3_{i-1/2,j}h_{i-1,j}$$

$$-h_{i,j}\left(b^3_{i,j+1/2} + b^3_{i,j-1/2} + b^3_{i+1/2,j} + b^3_{i-1/2,j}\right) = 0, \tag{0.2}$$

where the subscripts i and j are the discretized distance along the $x-$ and $y-$directions, respectively. The five–point finite difference stencil is shown in Figure 0.3. The aperture at the interface of two adjacent elements in the $x-$ and $y-$directions is obtained by employing the harmonic mean [*Reimus*, 1995; *James and Chrysikopoulos*, 2001b]

$$b^3_{i,j\pm1/2} = \frac{2b^3_{i,j}b^3_{i,j\pm1}}{b^3_{i,j} + b^3_{i,j\pm1}}, \tag{0.3}$$

$$b^3_{i\pm1/2,j} = \frac{2b^3_{i,j}b^3_{i\pm1,j}}{b^3_{i,j} + b^3_{i\pm1,j}}. \tag{0.4}$$
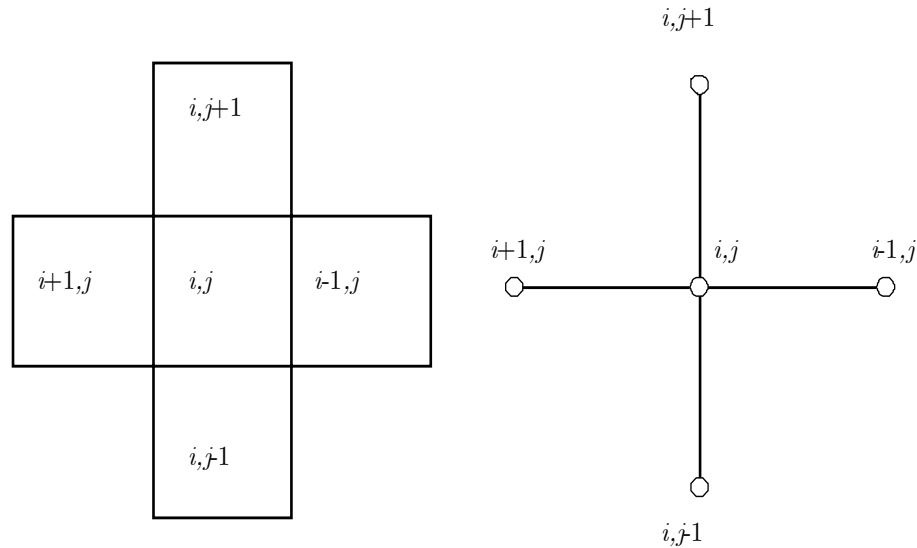
Figure 0.3: Five–point finite difference stencil.

Using the finite difference numerical approximation (0.2) for the solution of the

governing flow equation (0.1) for each node on the grid of the fracture plane results in

a set of linear equations with as many unknowns as the number of unspecified nodes

on the fracture grid [*Hoffman*, 1992, p. 825]. The resulting set of linear equations is

solved using a banded LU decomposition matrix solver algorithm [*Press et al.*, 1992,

p. 963]. Average velocity components in the x– and y–directions are then calculated

for every element from the steady–state volumetric fluxes by the following expressions:

$$\overline{u}_x = -\frac{\gamma b^2\left(x,y\right)}{12\mu}\frac{\partial h\left(x,y\right)}{\partial x},\tag{0.5}$$

$$\overline{u}_y = -\frac{\gamma b^2\left(x,y\right)}{12\mu}\frac{\partial h\left(x,y\right)}{\partial y},\tag{0.6}$$

where γ is the specific weight of water, and μ is the dynamic viscosity of water.

Second order accurate finite difference forms of (0.5) and (0.6) used in this analysis
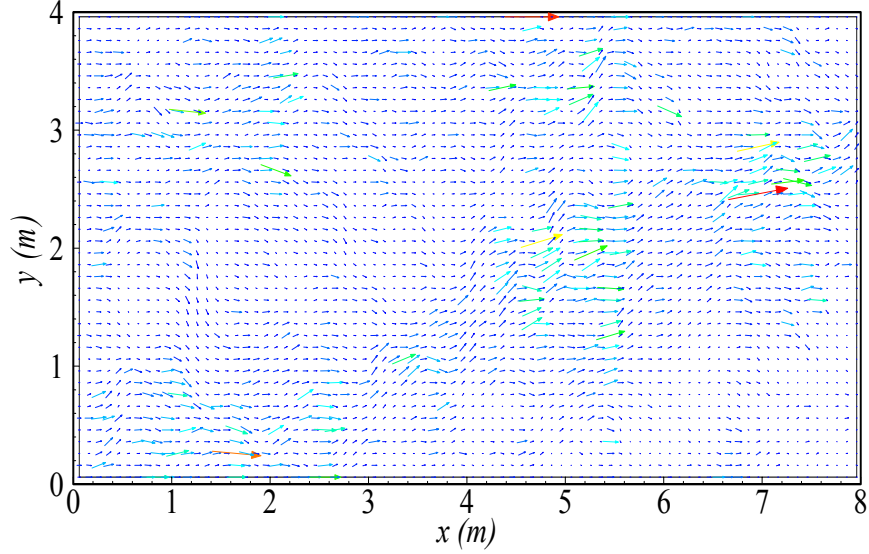
Figure 0.4: The velocity field in the variable aperture fracture shown in Figure 0.2. Arrow lengths are tangential and proportional to the local mean velocity.

are given as

$$\overline{u}_{x_{i,j}} = -\frac{\gamma b_{i,j}^2}{12\mu} \frac{h_{i+1,j} - h_{i-1,j}}{2\Delta x}, \tag{0.7}$$

$$\overline{u}_{y_{i,j}} = -\frac{\gamma b_{i,j}^2}{12\mu} \frac{h_{i,j+1} - h_{i,j-1}}{2\Delta y}. \tag{0.8}$$

Because the fluid flow is laminar, a parabolic velocity profile develops within each element; the velocities in the $x-$ and $y-$directions are functions of z and expressed as

$$u_x\left(x, y, z\right) = \overline{u}_x\left(x, y\right) \frac{3}{2} \left\{ 1 - 4 \left[\frac{z}{b\left(x, y\right)} \right]^2 \right\}, \tag{0.9}$$

$$u_y\left(x, y, z\right) = \overline{u}_y\left(x, y\right) \frac{3}{2} \left\{ 1 - 4 \left[\frac{z}{b\left(x, y\right)} \right]^2 \right\}. \tag{0.10}$$

There is no advective component in the $z-$direction, normal to the fracture surface. Equations (0.9) and (0.10) are consequences of the no slip boundary conditions at the fracture walls, and therefore functions of the spatial (x, y, z) location in the fracture.

The corresponding velocity field for the variable aperture fracture realization of Figure 0.2 is shown in the vector plot of Figure 0.4.

Zero fluxes at the upper and lower bounds ($y = 0$ m and $y = 4$ m) of the fracture are imposed by the boundary conditions employed in the solutions of (0.5) and (0.6), and insure conservation of mass in the system. In the event that a particle diffuses a distance past the upper or lower y boundary, it is reflected back into the fracture by an equal distance. Thus, particles may enter only at the left hand (upstream) boundary of the system, and exit at the right hand (downstream) boundary.

0.2.3 Time Step Selection

Both solution accuracy and computational efficiency must be considered when choosing the time step for a particle tracking algorithm. Unfortunately, improving solution accuracy compromises computational efficiency and vice versa. Increased accuracy is achieved by decreasing the time step to gain finer resolution of the particles' motion, while computational efficiency is improved by increasing the time step, thereby reducing the number of steps necessary to attain the desired solution. Thus, an appropriate balance between these two objectives must be struck that satisfies each to a reasonable degree. The challenge of selecting a single appropriate time step for both colloids and contaminants lies in their significantly different transport properties, particularly their diffusion coefficients, that differ by four orders of magnitude.
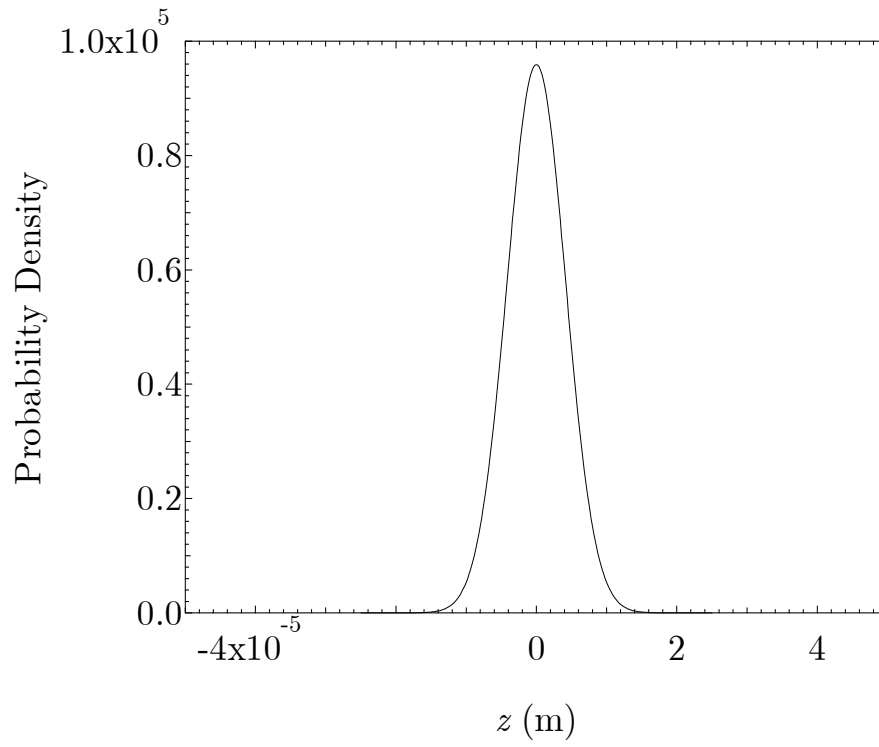
Figure 0.5: Probability distribution of z–locations for colloids diffusing through a time step $\Delta t = 100$ s released at $z = 0$ m.

The selection of the time step is based on colloid diffusion in the z–direction. A value is chosen such that a colloid released at $z = 0$ m (the center of the fracture) would be unlikely to diffuse more than 40% of the average aperture, $\bar{b}$, in a single time step. Figure 0.5 shows the probability density of final z–locations after one time step of $\Delta t = 100$ s for colloid particles released at $z = 0$ m. Note that the average aperture of the fracture, $\bar{b} = 5 \times 10^{-5}$ m, is represented by the left and right vertical axes and that 99% of the distribution lies between $\pm 1.4 \times 10^{-5}$ m, virtually insuring that the above criterion is met. Note that in Figure 0.5 the combination of the extremely small range along the x–axis and the fact that the area under a normalized

probability density curve is unity, results in the large peak of the distribution. This time step selection also insures that a colloid will never diffuse a distance sufficient to reflect from one wall, cross the fracture, and embed itself in the opposite wall.

When considering isotropic diffusion from a line source, the distribution is normal (centered about zero); with standard deviation, σ, proportional to $(\Delta t)^{1/2}$. Recall that the root mean square (RMS) value of the standard normal distribution, $Z(0,1)$, is equal to one and that colloid diffusion in the z–direction is estimated as

$$\Delta z = Z(0,1)\sqrt{2\mathcal{D}\Delta t}. \tag{0.11}$$

The RMS of the standard normal distribution may be defined as:

$$\text{RMS} = \sqrt{\frac{\sum\limits_{n=1}^{N}[Z(0,1)]^2}{N}} = 1; \tag{0.12}$$

the general expression for the standard deviation of any distribution is:

$$\sigma = \sqrt{\frac{\sum\limits_{n=1}^{N}(\overline{x}-x)^2}{N}}. \tag{0.13}$$

For the standard normal (Gaussian) distribution, $\mu_d = 0$ ($\overline{x} = 0$) and equations (0.12) and (0.13) are equivalent, i.e., $\sigma = \text{RMS}$. Multiplication of the RMS (or σ) by a constant, κ, scales the standard deviation of the distribution:

$$\sqrt{\frac{\sum\limits_{n=1}^{N}[\kappa Z(0,1)]^2}{N}} = \kappa. \tag{0.14}$$

Thus, according to (0.11), the standard deviation of the diffusion equation is equal to $\sqrt{2\mathcal{D}\Delta t}$, and σ is shown to be proportional to $(\Delta t)^{1/2}$.
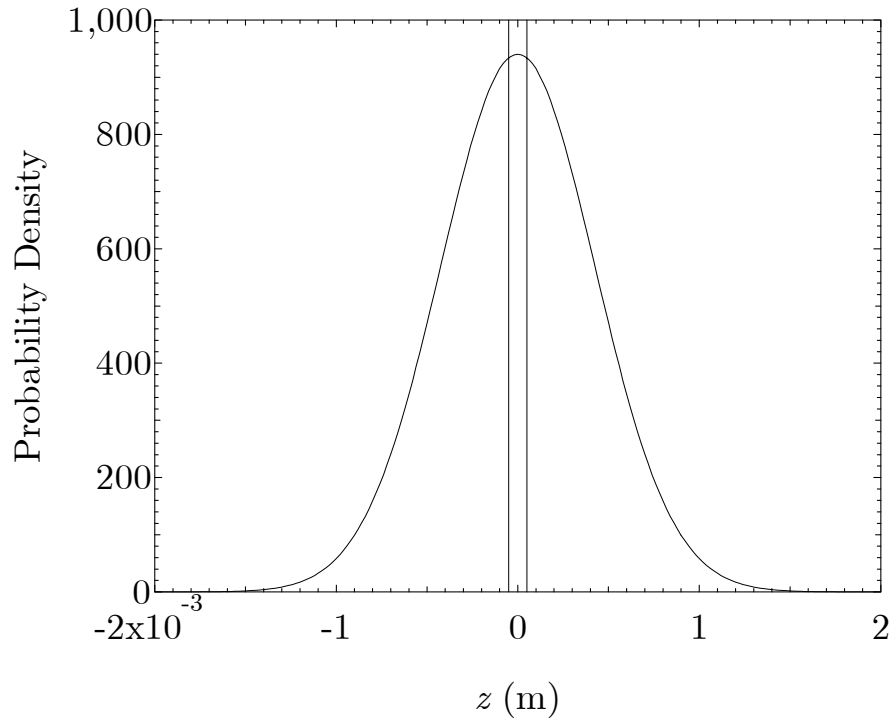
Figure 0.6: Probability distribution of z–locations for contaminants diffusing for a single time step of $\Delta t = 100$ s released at $z = 0$ m.

The Gaussian distribution has probability density [*Banks et al.*, 1996]

$$f\left(x\right) = \frac{1}{\sigma\sqrt{2\pi}}\exp\left[-\frac{1}{2}\left(\frac{z}{\sigma}\right)^2\right].$$

(0.15)

Recall that the mean diffusion distance is zero, yielding the probability density function in Figure 0.5 with form:

$$\Omega(z) = \frac{1}{\sqrt{2\mathcal{D}\Delta t}\sqrt{2\pi}}\exp\left[-\frac{1}{2}\left(\frac{z}{\sqrt{2\mathcal{D}\Delta t}}\right)^2\right].$$

(0.16)

For a contaminant particle, the time step appropriate for colloids does not limit the diffusive travel distance to 40% of the mean fracture aperture. Figure (0.6), is

obtained by substituting the contaminant diffusion coefficient in (0.16), and shows the probability density of final z–locations for a plume of contaminant particles released at $z = 0$ m, after a single time step of $\Delta t = 100$ s. The range of probable diffusion distances for contaminants extends far beyond the average fracture aperture, represented in Figure 0.6 by the two vertical lines near the origin, clearly illustrating that a time step deemed appropriate for colloids is highly impractical when applied to contaminants. Quantitatively, when the contaminant diffusion coefficient is substituted in (0.11) the resulting contaminant RMS diffusion distance is two orders of magnitude larger than that for colloids due to the four order of magnitude difference between the diffusion coefficients. Consequently, implementation of a single time step appropriate for a colloid is likely to cause a contaminant to diffuse deeply into the porous matrix.

To accurately track contaminant movement in the z–direction, the particle tracking time step should be four orders of magnitude smaller than the time step for colloids, $\Delta t = 0.01$ s. This time step, while providing good resolution of the movement of contaminant particles, is computationally costly, with implementation increasing the simulation time by approximately four orders of magnitude.

Because of the strict time step requirements for contaminants, they are modeled two–dimensionally, that is, only the x– and y–movements are determined by the particle tracking equations, with a time step of $\Delta t = 100$ s. Contaminant particles need not be tracked in the z–direction while flowing in the fracture, based on the

assumption that a contaminant plume travels with the local average fluid velocity.

0.2.4 Plume Descriptions

Two individual plumes with 5,000 contaminant and 5,000 colloid particles are released instantaneously ($t = 0$ s) at the inlet ($x = 0$ m) of the fracture. The colloid plume is assumed to be monodisperse with respect to size and species, with diameter $d_p = 5 \times 10^{-6}$ m. Each colloid particle is assigned a finite number of contaminant sorption sites. When all sorption sites on a colloid have been filled, that particle is removed from consideration for any further co–transport phenomena. The contaminant plume is composed of a single dissolved species of molecular size, and modeled as point particles, $d_p = 0$ m.

0.2.5 Initial Particle Placement

Figure 0.7 is a representative distribution of initial colloid locations ($x = 0$ m, $t = 0$ s), in the range of $0 \leq y \leq 0.8$ m. In these simulations, the colloid and contaminant plumes are introduced at the inlet side of the fracture flow domain ($x = 0$ m) and distributed according to the local volumetric flow rate as suggested by *Reimus* [1995, p. 93]. A discrete cumulative probability density function based on the volumetric flow rate into each inlet element of the fracture is constructed by summing all individual element flow rates at the fracture inlet and determining each element's contribution (probability) to the sum. Subsequently, a uniform random
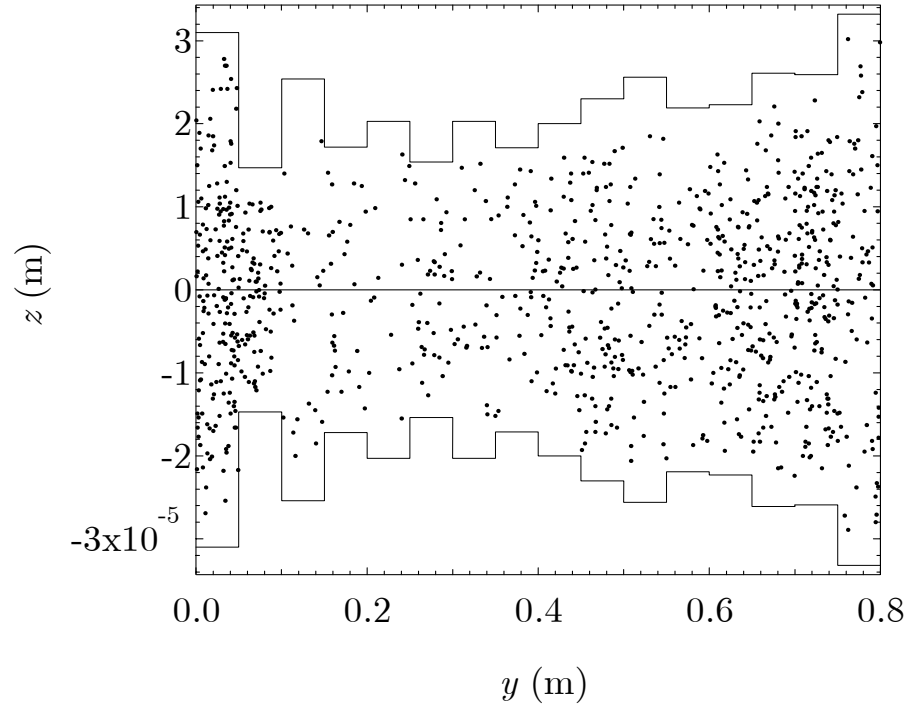
Figure 0.7: Initial colloid placement in the $x = 0$ m plane.

number between zero and one is generated for each particle. The random number's

placement in the cumulative distribution of the flow rates at the inlet designates the

corresponding entrance element. Once the element, j, is specified, a particle's exact

y–coordinate (in meters) is assigned by the equation:

$$y = \frac{(j-1) + Rn\,(0,1)}{50}, \tag{0.17}$$

where $Rn(0,1)$ is a uniformly distributed random number between 0 and 1. It is

assumed that the probability of a colloid entering a fracture element at a given z–

location (perpendicular to the fracture walls) is proportional to the flow rate at that

particular position. Consequently, the normalized probability of a colloid having a

starting position less than z is [*Reimus*, 1995; *James and Chrysikopoulos*, 2000]

$$P(z) = \frac{\int_{-b/2}^{z} U_{\max} \left[1 - 4\left(\frac{z}{b}\right)^2\right] dz}{\int_{-b/2}^{b/2} U_{\max} \left[1 - 4\left(\frac{z}{b}\right)^2\right] dz};$$

(0.18)

solution of this equation gives:

$$P(z) = -2\left[\frac{z}{b\,(0,y)}\right]^2 + \frac{3}{2}\frac{z}{b\,(0,y)} + \frac{1}{2}.$$

(0.19)

A uniform random number between zero and one is substituted for $P(z)$ in (0.19)

and the roots of the resulting polynomial in z are evaluated by Newton's Method.

Roots found outside of the range of $\pm b(0,y)/2$ are discarded due to the restriction on

colloid particles from entering the matrix. Thus, the centroid of the colloid must be

placed a distance of at least $d_p/2$ m from the fracture wall to insure that it is wholly

contained within the fracture.

0.3   Numerical Model

0.3.1   Particle Tracking

A particle tracking algorithm is used to track the movement of each particle in

the system. The position and status (freely moving within the fracture, sorbed to

the wall, time of elution, etc.) of each particle is updated each time step. This

method differs from finite difference and finite element solutions to the advection–

diffusion equation that calculate concentration as a function of time and space. These

techniques are subject to numerical dispersion due to truncation errors in their formulation. Provided that a sufficient number of particles are used in each simulation and enough simulations are performed, when the results are combined into an ensemble average to smooth the random noise inherent in a stochastic scheme, a particle tracking method used with an appropriate time step yields an excellent solution to the advection–diffusion equation.

As described above, the numerical model used in this research is three–dimensional for colloid particles, and two–dimensional for contaminant particles within the fracture. Recall that restrictions on time step magnitudes due to computational limitations prevent the contaminants from being tracked in the z–direction as the diffusion distance for a relatively small time step often results in a contaminant particle diffusing significantly into the fracture matrix.

Colloids are subject to advection, diffusion, and sorption onto the fracture walls. They may not diffuse into the surrounding porous matrix, based on the assumption that colloid size is greater than the pore size of the surrounding matrix [*Abdel-Salam and Chrysikopoulos*, 1995a]. Contaminants move through the fracture via advection and diffusion in the x– and y–directions; their transport is retarded via sorption onto the fracture walls and diffusion into and sorption onto the surrounding porous rock matrix. Contaminants may sorb onto colloid particles, thereby assuming the transport properties of the carrier colloid and exhibiting enhanced overall transport of the plume.

Colloids travel by advection in the $x-$ and $y-$directions according to the local parabolic velocity profiles given by (0.5) and (0.6), and diffuse isotropically in all directons. The general advective/dispersive particle tracking equations used for colloid particles are [*Thompson and Gelhar*, 1990; *James and Chrysikopoulos*, 2000]:

$$x^{m+1} = x^m + u_x\left(x^m, y^m, z^m\right)\Delta t + Z\left(0, 1\right)\sqrt{2\mathcal{D}\Delta t}, \qquad (0.20)$$

$$y^{m+1} = y^m + u_y\left(x^m, y^m, z^m\right)\Delta t + Z\left(0, 1\right)\sqrt{2\mathcal{D}\Delta t}, \qquad (0.21)$$

$$z^{m+1} = z^m + Z\left(0, 1\right)\sqrt{2\mathcal{D}\Delta t} \qquad (0.22)$$

where x^{m+1}, y^{m+1} and z^{m+1} are the coordinates of a particle at time level $m + 1$; u_x and u_y are the local interstitial $x-$ and $y-$velocities specified by (0.9) and (0.10) respectively; Δt is the time step; $Z\left(0, 1\right)$ is a random selection from the standard normal (Gaussian) distribution; and $\mathcal{D}$ is the diffusion coefficient. The diffusion coefficient for a colloid particle is calculated from the Stokes–Einstein equation [*Welty et al.*, 1984]:

$$\mathcal{D} = \frac{kT}{3\pi\mu d_p}, \qquad (0.23)$$

where k is Boltzmann's constant; and T is the absolute temperature of the interstitial fluid.

Upon colloid movement between fracture elements with different apertures, its new $z-$location must be determined. Here, a ratio, valid under creeping flow conditions in slowly converging or diverging channels, is employed that is a function of the former

and current apertures and the former z–location [*Haber and Brenner*, 1993]:

$$z_{\text{new}} = z_{\text{old}} \frac{b_{\text{new}}}{b_{\text{old}}}. \tag{0.24}$$

Colloids may travel either perpendicularly or diagonally between elements, however only the initial and final z–locations and apertures are employed in (0.24).

The particle tracking equations used for contaminant particles in the x– and y– directions are:

$$x^{m+1} = x^m + \overline{u}_x (x^m, y^m) \Delta t + Z(0, 1) \sqrt{2\mathcal{D}\Delta t}, \tag{0.25}$$

$$y^{m+1} = y^m + \overline{u}_y (x^m, y^m) \Delta t + Z(0, 1) \sqrt{2\mathcal{D}\Delta t}. \tag{0.26}$$

Note that contaminants are advected according to the average x– and y–velocities rather than by (0.9) and (0.10). The use of average velocities for contaminants is necessitated by the prohibitively small time step that would be required to accurately to track the particles in the z–direction. This approach is justified by their large molecular diffusion coefficient, and will be verified in the following section. A representative diffusion coefficient, $\mathcal{D} = 9.0 \times 10^{-10}$ m^2/s was chosen for a molecular sized contaminant diffusing in water at $T = 285$ K [*Welty et al.*, 1984].

If a particle diffuses beyond the zero flow boundaries at $y = 0$ m or $y = 4$ m it is reflected back into the fracture by a length equal to the distance from the boundary it would have reached, thereby preserving conservation of mass within the system. For example, if a particle's y–location after a time step is $y = 4.004$ m, the model automatically places it back in the fracture at $y = 3.996$ m, thus the model assumes

perfectly solid and 100% reflective boundaries.

0.3.2   Dispersion in a Fracture

0.3.2.1   Taylor Dispersion

The movement of a dissolved particle through a fracture is chiefly driven by axial advection and transverse molecular diffusion. Taylor dispersion, arising from the combination of molecular diffusion and a velocity gradient, is the result of the combined presence of molecular diffusion and a velocity gradient. According to the Stokes-Einstein equation, (0.23), the molecular diffusion coefficient is inversely proportional to the particle diameter, explaining the relatively large diffusivity of a soluble contaminant compared to a colloid. This property allows the contaminant to diffuse rapidly across the width of the fracture and frequently sample all velocities across the flow profile. A colloid particle in the same fracture however, with a much larger diameter and therefore a smaller diffusion coefficient, will experience less transverse diffusion and sample fewer streamlines, thus traveling at a nearly constant velocity for longer time intervals. Thus, a contaminant plume experiences a lesser degree of Taylor dispersion than a colloid plume in the same fracture. The molecular diffusion coefficient and the Taylor dispersion coefficient are inversely related as shown [*Taylor*, 1953]:

$$D_{\mathrm{Taylor}} = \mathcal{D} + \frac{2}{945} \frac{U_{\mathrm{max}}^2 b^2}{\mathcal{D}}.$$

(0.27)

Because a dissolved contaminant or solute rapidly diffuses across flow streamlines (z–direction), adopting local velocities along the way, it ultimately travels with the mean fluid velocity, decreasing axial spreading of the plume. A colloid's relatively small diffusion coefficient tends to keep it on a single streamline for a longer period of time, thus each colloid particle travels at a relatively constant velocity over a time interval, facilitating axial spreading of the plume due to the parabolic velocity profile. When combined in the particle tracking model, use of the Taylor dispersion coefficient and the average x– and y–velocities within each element for contaminant particles allow accurate determination of contaminant movement without the need to track contaminant movement in the z–direction, thus solving the problem of time step selection.

An effective dispersion coefficient has been derived that accounts for particle diameter [*James*, 2001]:

$$D_{\text{eff}} = \mathcal{D} + \frac{2}{945} \frac{U_{\text{max}}^2 b^2}{\mathcal{D}} \left(1 - \frac{d_p}{b} \right)^6.$$
(0.28)

Because of their finite size, colloids are excluded from the slower moving portions of the flow field, further differentiating their transport behavior from a dissolved species. It is important to note that size exclusion of colloids limits the ability of Equation (0.27) to accurately determine an appropriate Taylor dispersion coefficient due to its assumption that a particle may sample the entire flow profile. Accounting for size exclusion of colloids serves to decrease the effect of Taylor dispersion because colloids may not sample the full range of velocities across the fracture; size exclusion also

serves to increase the average velocity of a colloid plume.

The magnitude of the individual effect of Taylor dispersion on two non-reacting plumes, colloids and dissolved contaminants, is presented and discussed in detail for a uniform aperture fracture model. To illustrate the difference in the values of a molecular diffusion coefficient and a Taylor dispersion coefficient, consider a contaminant ($\mathcal{D}_{\text{cont}} = 9 \times 10^{-10}$ m^2/s) and a colloid ($d_p = 1 \times 10^{-6}$ m, $\mathcal{D}_{\text{coll}} = 8.65 \times 10^{-14}$ m^2/s) flowing in a fracture ($\overline{u} = 1 \times 10^{-5}$ m/s, $\overline{b} = 5 \times 10^{-5}$ m). The Taylor dispersion coefficient for the contaminant is $D_{\text{cont}} = 9.22 \times 10^{-10}$ m^2/s; the effective Taylor dispersion coefficient for the colloid is $D_{\text{eff}_{\text{coll}}} = 9.90 \times 10^{-8}$ m^2/s. The value of the Taylor dispersion coefficient for a soluble contaminant does not depart significantly from the molecular diffusion coefficient, but the change from diffusion to dispersion coefficient for a colloid increases the coefficient by 6 orders of magnitude. Two conclusions may be drawn from this example, first it is shown that use of the Taylor dispersion coefficient for a contaminant does not significantly impact the transport of the plume; second the magnitude of the Taylor dispersion coefficient is shown to be far greater for a colloid than a soluble contaminant, a result that directly correlates to the extent of Taylor dispersion experienced by the individual species.

0.3.2.2   Mechanical Dispersion

In systems of variable aperture fractures or fracture networks, mechanical dispersion is the primary mechanism contributing to spreading of a plume of particles. A fluid will preferentially flow through a channel that offers the least resistance, specifically paths that exhibit the widest apertures. A particle that flows along these preferential flow paths will experience a decreased residence time within the fracture, exiting the system far earlier than a particle that travels through a narrower and therefore slower moving section of the same fracture. A range of residence times corresponding to various paths along a fracture may result in a wide range of elution times for a plume of particles.

An increase in the heterogeneity of fracture apertures, resulting in increasingly tortuous flow paths, is yet another factor that may contribute to mechanical dispersion. The effects of mechanical dispersion on a contaminant and a colloid plume are presented using breakthrough curves from a model incorporating a variable aperture fracture by comparison with a results from a uniform aperture simulation in which Taylor dispersion is the main driving force for spreading of a plume.

0.3.3   Matrix Diffusion

Colloid particles were excluded from the porous matrix because of size constraints, (i.e., the particles are larger than the pores in the fractured medium) [*Reimus*, 1995]. The probability of a contaminant diffusing from the fracture into the surrounding

matrix during a time step Δt was given by *Liu et al.* [2000] as:

$$P_{fm} = \frac{F_{fm}\Delta t}{V_f C_f} \tag{0.29}$$

where F_{fm} is the solute transport rate from the fracture element to the matrix, V_f is the liquid volume in the fracture, defined as the grid block volume multiplied by the porosity and volumetric liquid water saturation corresponding to the continuum, and C_f is the solute concentration in the fracture.

The probability of diffusing into the surrounding matrix is determined for each contaminant that is moving freely within the fracture during the current time step. A uniformly distributed random number between zero and one is generated and compared with the diffusion probability, P_{fm}; if the random number is less than P_{fm}, the particle will diffuse into the fracture matrix during that time step, otherwise, it will remain in the fracture.

After a particle successfully diffuses into the porous matrix, the particle tracking model records its movement in the x–, y–, and z–directions, becoming fully three–dimensional for contmainants within the surrounding media. Due to the abrupt spatial variance in both the diffusion coefficient and porosity between the fracture and the matrix it becomes necessary to subject it to diffusive transport as well as two additional deterministic velocities within a specified distance from the fracture–wall interface, termed the transition layer. *Reimus* [1995] determined that failure to incorporate these terms in the particle tracking equation for contaminants within the porous matrix would result in false accumulation of particles in stagnant and/or low

porosity zones within the flow system. These velocities are expressed as:

$$U_{\mathcal{D}} = (\nabla \cdot \mathcal{D}) , \tag{0.30}$$

$$U_{\theta} = \mathcal{D} (\nabla \cdot \ln \theta) . \tag{0.31}$$

When these terms are incorporated, the model may be considered to exhibit three regions, symmetric about the center of the fracture ($z = 0$ m), each governed by a unique set of particle tracking equations. These regions are: (1), the fracture void space where contaminants and colloids are free to undergo advection and diffusion according to their respective particle tracking equations using the Taylor dispersion coefficient, (0.25) and (0.26); (2), a pair of transition layers that begin at the upper and lower fracture walls, ($z = \pm b(x, y)/2$ m), where the diffusivity and porosity decrease linearly from the values within the fracture ($\mathcal{D}_{\text{cont}} = 9.0 \times 10^{-10}$ m^2/s and $\theta = 1.0$) to the values inside the deep matrix ($\mathcal{D}_{\text{matrix}} = \theta \mathcal{D}_{\text{cont}} = 9.0 \times 10^{-10}$ m^2/s and $\theta = 0.1$) according to (0.30) and (0.31) respectively; and (3), the deep porous matrix, beyond the transition layer where the diffusion of the particle is governed by only the diffusive term, with the Taylor dispersion coefficient multiplied by the matrix porosity, $\theta = 0.1$. The dependence of the contaminant diffusion coefficient on the z–location is illustrated in Figure 0.8.

Inspection of the slope of the transition layer section of Figure 0.8, or the deterministic expressions, (0.30) and (0.31), reveals that both terms are positive in the direction toward the fracture. Once a contaminant has diffused into the rock matrix, it is assigned a z_{matrix}–location within the matrix of $z_{\text{matrix}} = 0.000005$ m, where
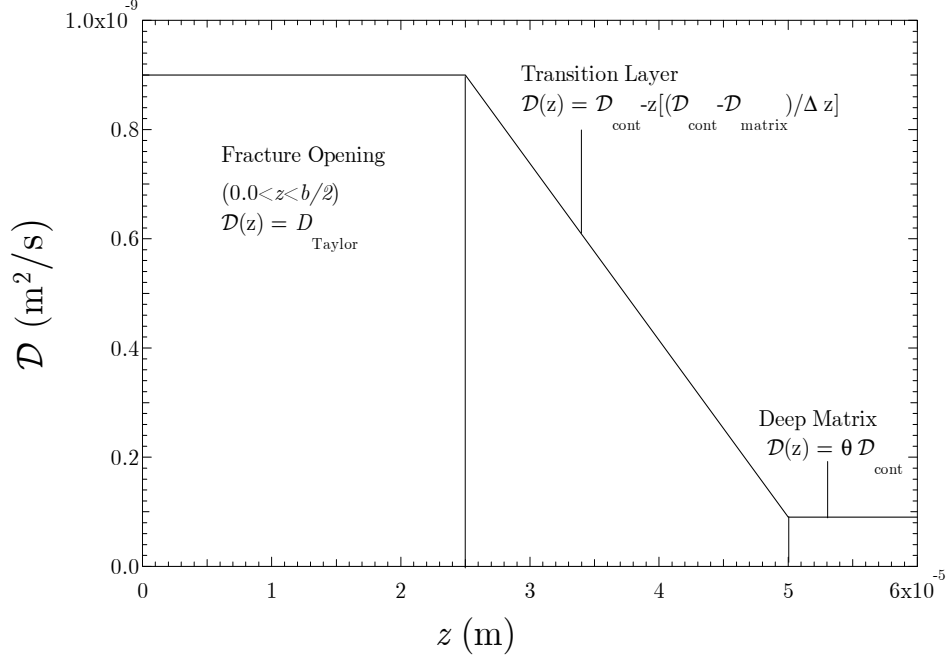
Figure 0.8: Contaminant diffusion coefficient in the fracture, transition layer and deep porous matrix.

$z_{\mathrm{matrix}} = 0$ m at the fracture–matrix boundary. A contaminant that diffuses into the matrix by (0.29) becomes subject to the transition layer particle tracking equation, in which only the diffusive term may serve to move the particle further into the matrix. As long as the contaminant is in the transition layer of the matrix, (0.30) and (0.31) will move it in the direction of the fracture with each time step; serving to eliminate false accumulation of contaminants within the matrix. The complete particle tracking equations within the transition layer are:

$$x^{m+1} = x^m + Z\left(0, 1\right) \sqrt{2\theta \mathcal{D}_{\mathrm{Taylor}} \Delta t}, \tag{0.32}$$

$$y^{m+1} = y^m + Z\left(0, 1\right) \sqrt{2\theta \mathcal{D}_{\mathrm{Taylor}} \Delta t}, \tag{0.33}$$

$$z^{m+1} = z^m + Z\left(0,1\right)\sqrt{2\theta\mathcal{D}_{\text{Taylor}}\Delta t} + \left(\nabla \cdot \mathcal{D}_{\text{Taylor}}\right)\Delta t + \mathcal{D}_{\text{Taylor}}\left(\nabla \ln \theta\right)\Delta t, \quad (0.34)$$

and in the deep porous matrix, beyond the transition layer:

$$x^{m+1} = x^m + Z\left(0,1\right)\sqrt{2\theta\mathcal{D}_{\text{Taylor}}\Delta t}, \qquad (0.35)$$

$$y^{m+1} = y^m + Z\left(0,1\right)\sqrt{2\theta\mathcal{D}_{\text{Taylor}}\Delta t}, \qquad (0.36)$$

$$z^{m+1} = z^m + Z\left(0,1\right)\sqrt{2\theta\mathcal{D}_{\text{Taylor}}\Delta t}. \qquad (0.37)$$

In the event that a contaminant particle diffuses out of the matrix, its z_{matrix} value becomes negative and its transport is once again governed by the original contaminant particle tracking equations, (0.25) and (0.26).

0.3.4 Fracture Wall Deposition

0.3.4.1 Colloids

When a colloid encounters a fracture wall, it either reflects back into the fracture, or it attaches to the wall. The probability, p, of colloid deposition onto fracture walls is governed by an equation derived from the Boltzmann law [*Adamczyk et al.*, 1991; *James*, 2001]

$$p = \exp\left(-\frac{\Phi}{kT}\right) F\left(n^*\left(t, x, y\right)\right), \qquad (0.38)$$

where Φ is the repulsive energy of interaction between the particle and the fracture surface. A standard value of $\Phi = 10kT$ joules is suggested by [*Adamczyk et al.*, 1992a] and is used for all colloids in this model. $n^*\left(t, x, y\right)$ is the time and space dependent number of previously sorbed colloids per unit fracture element.

The linear, normalized dynamic blocking function (DBF), $F\left(n^{*}\left(t, x, y\right)\right)$, accounts for the area occupied by previously deposited colloids, and, as coverage of the fracture wall increases, increasingly limits the probability of both colloid and contaminant fracture wall deposition. Sorbed contaminants are assumed to have an insignificant impact on the value of the DBF due to their infinitesimally small size. The value of $F\left(n^{*}\right)$ for a clean fracture (no previous deposition) is unity, and approaches zero as a fracture wall nears monolayer coverage. This insures that in the event of complete monolayer coverage of the fracture walls, further sorption is impossible [*Song and Elimelech*, 1994; *Chrysikopoulos and Abdel-Salam*, 1997]. The DBF is expressed as [*Elimelech et al.*, 1995]:

$$F\left(n^{*}\left(t, x, y\right)\right) = \frac{\epsilon_{\max} - \epsilon\left(t, x, y\right)}{\epsilon_{\max}}, \quad (0.39)$$

where

$$\epsilon\left(t, x, y\right) = A_{p} n^{*}\left(t, x, y\right) \quad (0.40)$$

and

$$\epsilon_{\max} = \frac{1}{\beta}, \quad (0.41)$$

where $A_{p} = \pi d_{p}^{2}/4$ is the cross–sectional area of a colloid particle and $\beta\left(\geq 1\right)$ is a dimensionless parameter representing the ratio of the fracture surface area blocked by a deposited colloid particle to the projected area of the particle (shadow effect). Thus, with each colloid particle that is deposited onto the fracture surface, an area of the fracture wall equal to the profile of the colloid plus an added area due to a

hydrodynamic shadow effect is removed from the area available for further particle deposition [*Rajagopalan and Chu*, 1981]. The DBF is multiplied by $\exp(-\Phi/kT)$, the probability of attachment to a clean fracture wall, as shown in (0.38) to yield the total sorption probability per wall encounter. To ultimately determine whether a particle will be deposited onto the wall or be reflected back into the fracture each time a wall encounter is recorded, a uniformly distributed random number between zero and one is generated and compared to the time, location and concentration dependent sorption probability, (0.38). If the random number is less than the sorption probability, the colloid attaches to the wall, and $F(n^*)$ is updated for that fracture element. Otherwise, the particle is reflected back into the fracture.

0.3.4.2 Contaminants

A wall encounter by a contaminant may result in deposition onto the wall, diffusion into the porous matrix or reflection back into the fracture. Because the model does not track the motion of the contaminants in the z–direction, and therefore cannot count the number of wall encounters in a time step, it is necessary to use an expression to calculate the probability of contaminant wall sorption as a function of the time step:

$$P_{\text{cont}}(z) = 4\exp(-\frac{\Phi}{kT})\frac{\sqrt{\pi\mathcal{D}\Delta t}}{b(x,y)}\text{erf}\frac{(b(x,y))}{4\sqrt{\mathcal{D}\Delta t}}. \tag{0.42}$$

Once the probability of contaminant sorption is determined, the model follows a process that is analogous to colloid wall sorption. The probability is multiplied by

the DBF for the particular fracture element and compared to a uniformly distributed random number between zero and one. If the random number is less than the probability, the particle is deposited on the fracture wall and removed from further transport calculations; otherwise it is reflected back into the fracture. The DBF is not affected by a contaminant sorption phenomenon; it is assumed that the small relative size of a contaminant to a colloid would have a negligible effect on its value.

0.3.5 Particle–particle Sorption

An irreversible first-order kinetic sorption model suggested by (reference–Fetter),

$$\frac{\partial C^* (x, y)}{\partial t} = K_n C (x, y), \tag{0.43}$$

is modified for use in the particle tracking model. In this equation, $C^*(x, y)$ (kg/m^2) is the concentration of sorbed contaminants, $C(x, y)$ (kg/m^3) is the contaminant concentration, and K_n (m/s) is a first–order sorption rate constant. Because a particle tracking model determines particle number per fracture element rather than particle mass per volume, (0.43) was modified as follows:

$$\frac{\partial C^* (x, y)}{\partial t} = K_n \frac{C (x, y)}{b (x, y)}, \tag{0.44}$$

where now $C^*(x, y)$ (number/m^2) is the maximum number of contaminants that may undergo cotransport in a particular fracture element, $C(x, y)$ is the number of contaminants in an element, K_n is still the first–order sorption constant, and $b(x, y)$ (m) is the aperture of the particular fracture element. The number of contaminants expected

to undergo cotransport in a particular fracture element is inversely proportional the aperture of that element (i.e. the same number of contaminants in a small aperture element vs. a larger aperture element results in greater particle density, thus more potential sorption phenomena). For this reason, the factor $b(x, y)$ is used to transform the equation to contaminant number per element from contaminant mass per volume. The sorption rate constant, K_n, effectively measures the affinity of the two species for one another. The sensitivity of the model to the value of K_n is extensively investigated and adjusted to account for and explore the effects of varying degrees of attraction or repulsion based upon the characteristics of the contaminant and colloid species under consideration.

Equation (0.44) is separated and integrated to determine the maximum change in the number of sorbed contaminants in an element during a time step:

$$\Delta C^* (x, y) = K_n \frac{C (x, y)}{b (x, y)} \Delta t. \tag{0.45}$$

This equation gives the change in the number of cotransporting contaminants per element per time step. The result is then compared with the number of cotransporting contaminants in the corresponding element at the previous time level. Because desorption of contaminants is not considered, if the new number of cotransportng contaminants is negative, the model ignores the result and no cotransport phenomena occur.

Once the number of contaminants predicted to sorb onto colloid particles in each fracture element during a time step is determined, it is necessary to choose the colloid

particle to which the contaminant attaches. The number of sorption phenomena predicted to occur per time step and per fracture element is limited by the number of available sorption sites on the colloids in that element. To preserve spatial continuity, the contaminant particle can sorb only onto a colloid particle that is in the same fracture element. If a suitable colloid particle is found, i.e., a colloid with available sorption sites that is within the same element, the contaminant will sorb onto it and assume its transport properties. Once a contaminant particle attaches to a colloid, its new x– and y–location are updated according to the movement of the colloid to which it is attached. The contaminant is now prevented from diffusing into the porous matrix, and will only sorb onto the fracture wall if the carrier colloid is deposited. The transport properties of the colloid are unaltered by the contaminant on its surface. Once a contaminant sorbs onto a colloid, the number of available sorption sites for that particle is reduced by one until all of the sites are occupied. In the event that there are insufficient colloid particles with available sorption sites within an element, the contaminant particle does not sorb onto a colloid, but rather continues moving freely within the fracture.

Contaminants may also sorb onto colloids that have been deposited on the fracture walls. An equation analogous to (0.45) is used to predict the change in the number of contaminants sorbed onto deposited colloids using a new sorption rate constant, K_n^*, equal to $K_n/2$.

Table 0.1: Constant model parameters and values.

Parameter	Value	Reference
$\mathcal{D}_{\text{cont}}$	9.0×10^{-10} m^2/s	*Welty et al.* [1984]
$\mathcal{D}_{\text{coll}}$	8.65×10^{-14} m^2/s	*Welty et al.* [1984]
$\mathcal{D}_{\text{matrix}}$	9.0×10^{-11} m^2/s	*Reimus* [1995]; *James and Chrysikopoulos* [1999]
d_p	5×10^{-6} m	
θ	0.1	*James and Chrysikopoulos* [1999]
$\overline{b}$	5×10^{-5} m	*James and Chrysikopoulos* [1999]
$\Delta x, \Delta y$	5 cm	
Δt	100 s	

Table 0.2: Model variables and corresponding ranges.

Parameter	Range	Reference
Φ_{coll}	$0, \exp(-10)$	*Adamczyk et al.* [1992b]
Φ_{cont}	$0 - \exp(-10)$	*Adamczyk et al.* [1992b]
K_n	$0 - 5 \times 10^{-}8$	
sorption sites/colloid	$0, 1, 4$	

0.3.6 Model Parameters

The study of particle movement and reaction in a subsurface fracture incorporates the use of many model parameters. Because of the vast number of variables it was necessary to limit the scope of this research by selecting the parameters most likely to impact co–transport behavior. The model parameters that were held constant throughout this work are listed in Table 1; Table 2 presents the ranges of the parameters that were allowed to vary.

0.4 Numerical Simulations and Results

0.4.1 Uniform Aperture Fracture

The simplest particle tracking model studied is of a saturated fracture with uniform aperture, $b = 5 \times 10^{-5}$ m and an average velocity of $\overline{u} = 6 \times 10^{-5}$ m/s. The value of the Reynolds number, $Re = \rho \overline{u} b / \mu$, is 2.3×10^{-3}, well within the laminar range. Thus the fluid flow is characterized by a parabolic (Poiseuille) velocity profile. In this model variation, advection and diffusion (leading to Taylor dispersion) are the important transport mechanisms. Figure 0.9 shows a pair of breakthrough curves for two nonreacting plumes, one composed of colloids and the other of aqueous contaminants. Inspection of the breakthrough curves from this simplified model provides information about the basic transport behavior of each plume before additional model parameters are implemented. These curves are also used as references for comparison with results from more complicated models.

Note that constituents of the colloid plume are the first to reach the end of the fracture. This is a direct result of the size exclusion effect, otherwise known as hydrodynamic chromatography, which serves to accelerate the overall velocity of the plume [*Small*, 1974], and Taylor dispersion, which affects axial spreading. Because colloids can come only as close as $d_p/2$ m to the fracture walls and because colloids travel with the velocity found at their centroids, they are excluded from the slowest portions of the velocity profile. This results in an average colloid velocity greater
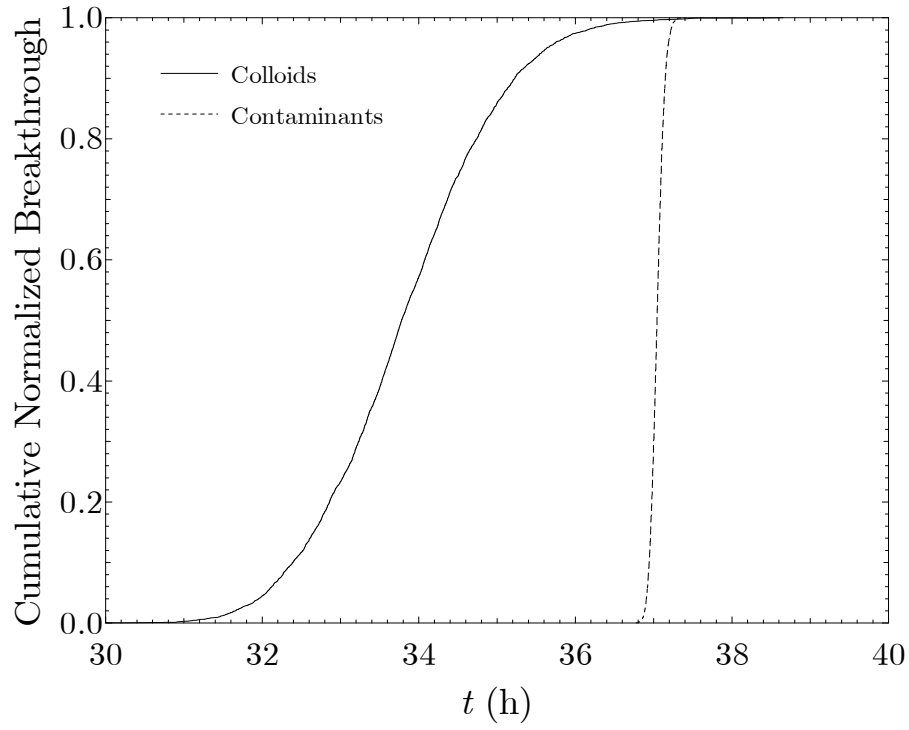
Figure 0.9: Colloid and contaminant breakthrough curves in a uniform aperture fracture.

than the average flow velocity. The average flow velocity within the fracture is found by integrating the expression for the velocity profile, (0.5), across the aperture, and dividing by the aperture,

$$
\begin{aligned}
\overline{U} &= \frac{1}{b} \int_{-b/2}^{b/2} u_z\left(z\right) dz \\
&= \frac{2}{3} U_{\text{max}}.
\end{aligned}
\tag{0.46}
$$

To find the average or effective velocity of a colloid particle, the limits of integration and the normalizing factor are adjusted to account for the particle's size [*James*,

2001]:

$$U_{\text{eff}} = \frac{1}{b - d_p} \int_{\frac{-b+d_p}{2}}^{\frac{b-d_p}{2}} u_z(z)dz$$

$$= \frac{2}{3}U_{\text{max}} \left[1 + \frac{d_p}{b} - \frac{1}{2}\left(\frac{d_p}{b}\right)^2 \right]. \tag{0.47}$$

The preceding equation is a function of the fracture aperture that is available to a colloid. Thus, the average velocity experienced by a colloid plume increases with increasing colloid diameter to aperture ratio [*James and Chrysikopoulos*, 2001a]. The effective velocity of a colloid plume is confirmed by examining the average elution times of each plume. The average elution time of the colloid plume is 33.8 hours; the average elution time of the contaminant plume is 37.0 hours, corresponding to average velocities of 6.57×10^{-5} m/s and 6.0×10^{-5} m/s respectively. Note that the effective velocity of the colloid plume ($d_p = 5 \times 10^{-6}$) from (0.47) is also 6.57×10^{-5} m/s.

The second important characteristic of note in Figure 0.9 is the difference in slopes of the breakthrough curves. The contaminant breakthrough curve is significantly steeper than the colloid curve, indicating less axial spreading of the contaminant plume. This is due to the more pronounced effect of Taylor dispersion on the colloid plume. The molecular diffusion coefficients of the two plumes differ by four orders of magnitude, with the larger diffusion coefficient belonging to the contaminant plume (recall that the diffusion coefficient is inversely proportional to the diameter). However, it was shown in (0.27) that the Taylor dispersion coefficient of the contaminant
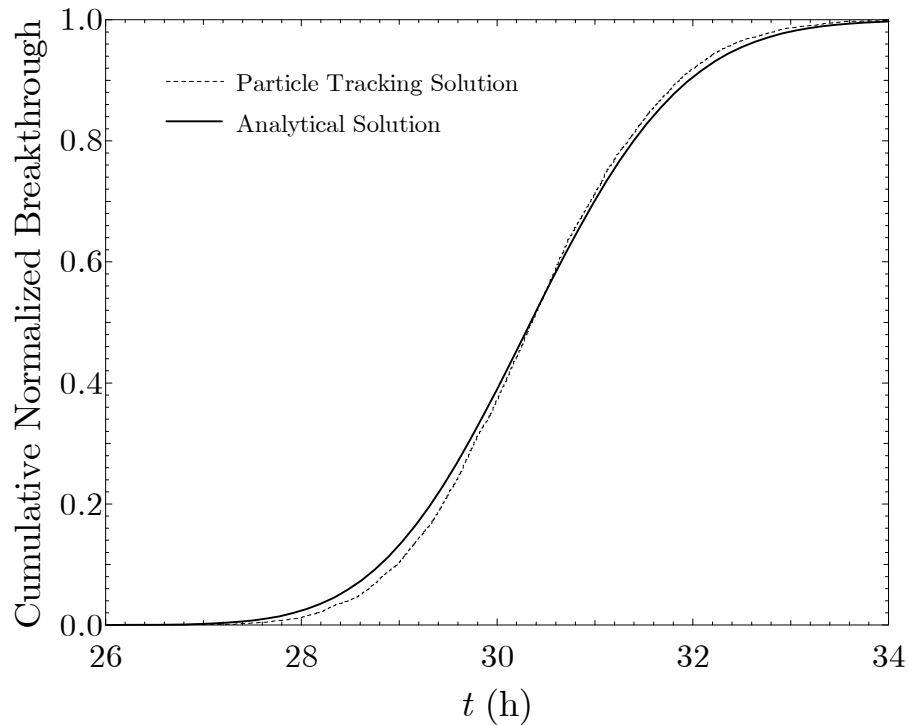
Figure 0.10: Comparison of analytically and numerically derived colloid breakthrough curves in a uniform aperture fracture, $b = 5 \times 10^{-5}$ m, $\overline{u}_x = 6 \times 10^{-5}$ m/s, $d_p = 5 \times 10^{-6}$ m.

plume is virtually the same as its diffusion coefficient, while the dispersion coefficient of a colloid is six orders of magnitude larger than its molecular diffusion coefficient.

Figure (0.10) is a comparison of two breakthrough curves for a plume of colloid particles, one curve obtained using an analytical solution to the transport equation in a uniform aperture fracture [*James and Chrysikopoulos*, 1999],

$$\overline{n}(x,t) = \frac{n_o}{(4\pi \mathcal{D}_{\text{eff}}t)^{1/2}} \exp\left[-\frac{(x - U_{\text{eff}}t)^2}{4\mathcal{D}_{\text{eff}}t}\right], \tag{0.48}$$

and the other from a particle tracking algorithm incorporating both molecular diffusion and size exclusion. Excellent agreement is shown between the two solutions,
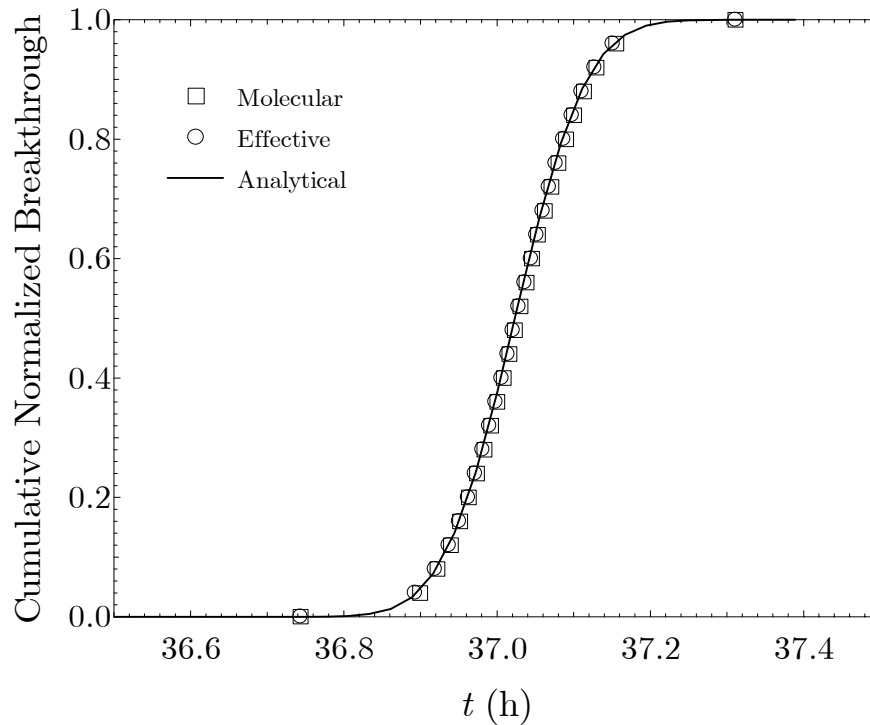
Figure 0.11: Analytically and numerically derived contaminant breakthrough curves in a uniform aperture fracture, $b = 5 \times 10^{-5}$ m, $\overline{u}_x = 6 \times 10^{-5}$ m/s.

indicating the degree of accuracy of the particle tracking model.

Figure 0.11 compares contaminant breakthrough curves obtained using three methods: an analytical solution, a particle tracking algorithm using a time step small enough ($\Delta t = 0.1$ s) to track the contaminants in the z–direction, and a particle tracking algorithm using the Taylor dispersion coefficient, average velocity, and a time step of $\Delta t = 100$ s. Once again, the agreement between the solutions illustrates the accuracy of the particle tracking model. This figure also supports the assertion that modeling contaminant transport using the effective dispersion coefficient, the average local velocity, and a large time step will provide accurate results.
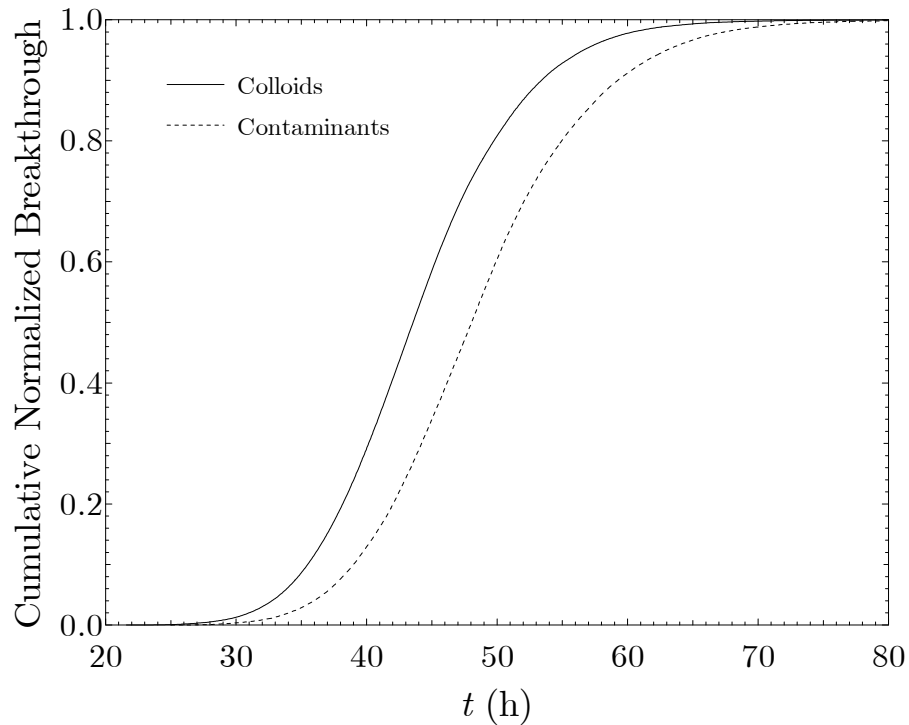
Figure 0.12: Colloid and contaminant breakthrough curves in a variable aperture fracture.

0.4.2 Variable Aperture Fracture

In this section, colloid and contaminant transport in a variable aperture fracture is investigated and compared to the results from the uniform aperture model. Figure 0.12 shows ensemble averaged breakthrough curves of two nonreactive plumes, colloids and contaminants, traveling through a variable aperture fracture under the influence of advection, diffusion, and dispersion. Both breakthrough curves exhibit elongation when compared to curves from the uniform aperture model of Figure 0.9 due to the influence of mechanical dispersion arising from the flow field. In a variable aperture fracture, water preferentially flows along the least resistive pathway,

i.e. the path where the fracture elements are widest (see Figures 0.2 and 0.4). The tortuosity of these preferential pathways combined with diffusion across streamlines causes spreading, or mechanical dispersion. It is interestng to note that the slopes of the curves are similar, indicating that mechanical dispersion in a variable aperture fracture has a more pronounced effect than Taylor dispersion. This may be explained by taking the variability of fracture apertures sampled by the particles as they travel through the fracture into account; the variety of z–locations and therefore velocities experienced by a particle as it crosses fracture element boundaries of differing apertures produces a scenario similar to Taylor dispersion, with the difference that both plumes are equally affected, as shown by the similarity in the slopes of the breakthrough curves. However, the colloid plume exits the fracture significantly ahead of the contaminant plume, indicating that size exclusion of colloids is still an important factor to consider in their transport.

0.4.3 Wall Deposition

The wall deposition parameter, Φ, was varied for a set of simulations to determine its influence on the total number of particles exiting the fracture. Figure 0.13 shows the resulting breakthrough curves. As expected, increasing the value of Φ, and thereby increasing the value of the sorption probability function, results in a decreased fraction of particles eluted. Each simulation starts with a fracture surface free of deposited colloids, and the dynamic blocking function is updated with each colloid sorption
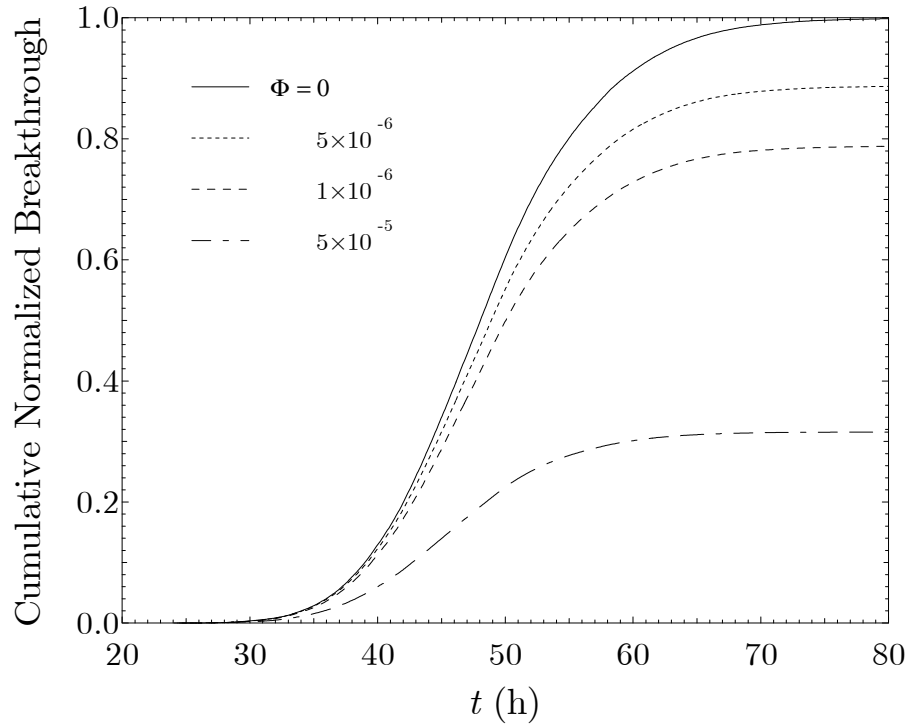
Figure 0.13: Contaminant breakthrough curves showing the effect of increasing the wall deposition parameter, Φ.

event. However, due to the very small size of the colloid particles relative to the surface area of the fracture and computational limitations on the total number of particles in a plume, the DBF never reached a value that significantly affected the sorption probability.

0.4.4 Matrix Diffusion

When matrix diffusion of contaminant particles is implemented in the model, significant retardation of the contaminant plume transport is shown in the corresponding breakthrough curve in Figure 0.14. Over long times, many of the particles diffuse back
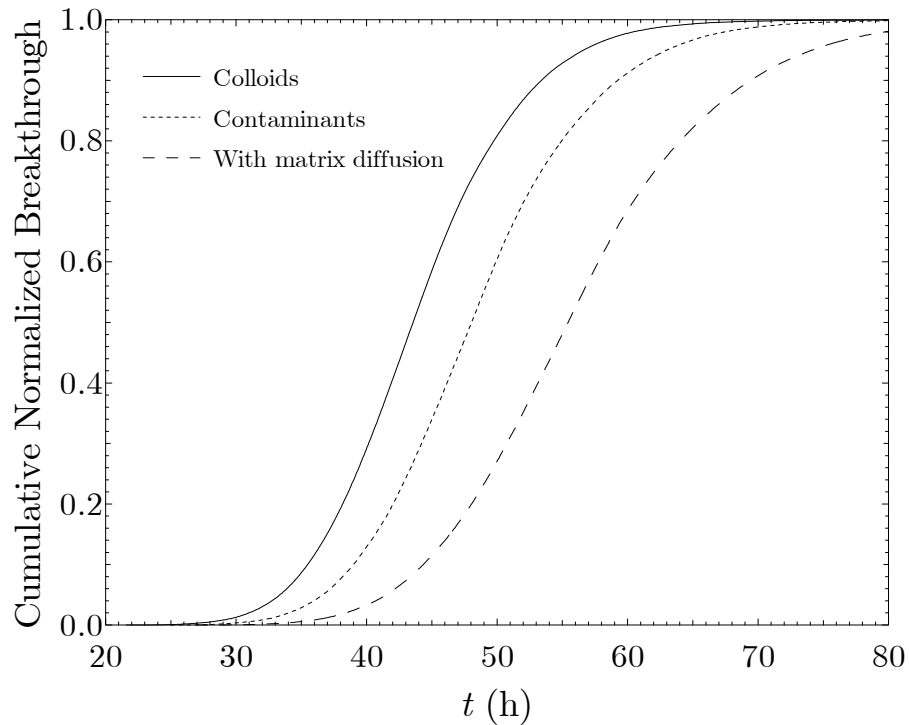
Figure 0.14: Colloid and contaminant breakthrough curves illustrating the retardation effect of matrix diffusion.

into the fracture, although some remain in the matrix. Under these conditions, as the plume passes through the fracture, the concentration gradient between the fracture and the rock matrix drives contaminants into the rock matrix in an attempt to achieve equilibrium. Once the bulk of the plume has passed and the direction of the concentration gradient has reversed, contaminants tend to emerge from the matrix and resume their flow toward the end of the fracture. This results in tailing of the breakthrough curves because plume constituents that have entered and exited the matrix have significantly increased residence time. When deposition of contaminants onto either fracture or matrix walls is included in the model the effect of matrix
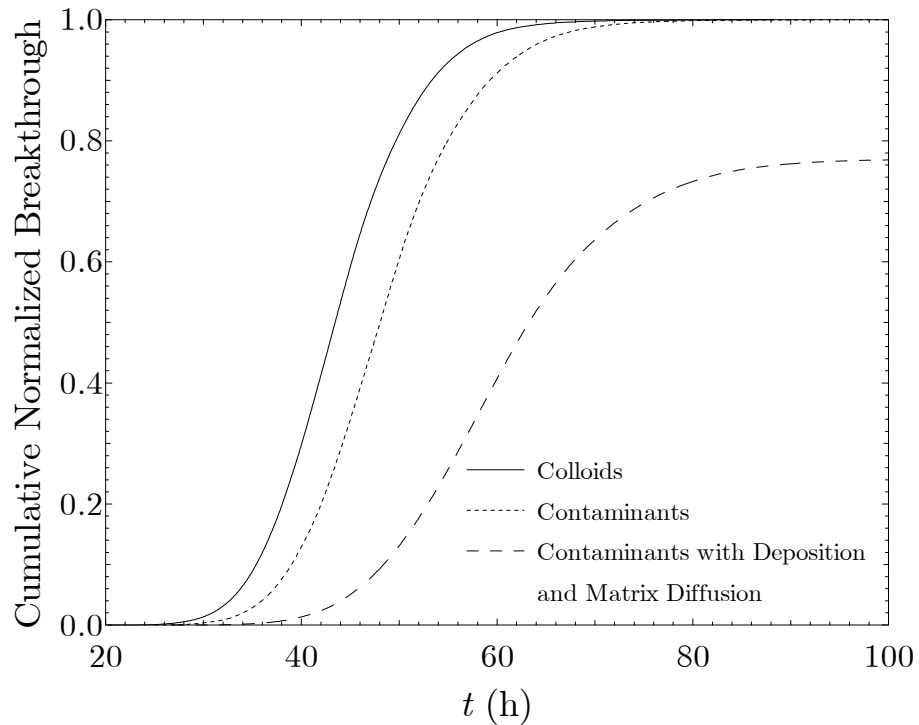
Figure 0.15: Colloid and contaminant breakthrough curves illustrating the combined effect of fracture wall deposition and matrix diffusion.

diffusion is vastly increased, as shown in the following section.

0.4.5   Wall Deposition and Matrix Diffusion

The combined effects of wall sorption, or deposition, and matrix diffusion, the two processes that serve to retard the transport of a contaminant plume as it travels through a fracture, are illustrated in Figure 0.15. A reference curve (no wall deposition or matrix diffusion), showing earlier breakthrough of the contaminant plume is included for comparison with the combined wall deposition and matrix diffusion model results.
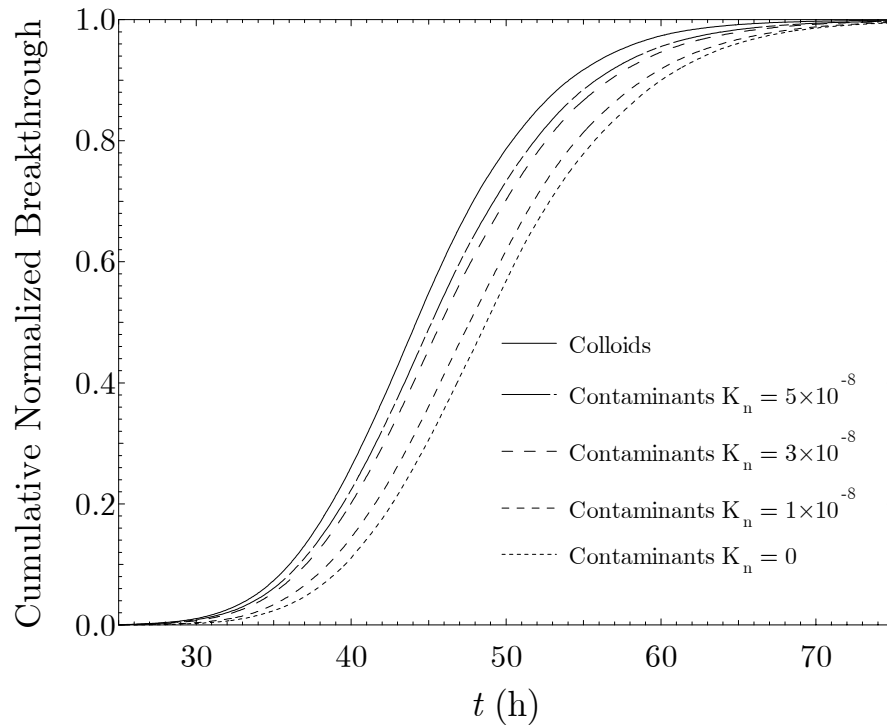
Figure 0.16: Colloid and contaminant breakthrough curves showing the effect of variation of the co–transport parameter, K_n.

The breakthrough curve in Figure 0.15 from a model including both matrix diffusion and fracture wall deposition illustrates the extensive retardation experienced by a plume under these conditions. In this simulation, the wall deposition parameter was $\Phi = 5 \times 10^{-6}$; comparison with the corresponding curve in Figure 0.13 shows that significantly fewer contaminants reach the end of the fracture for the same value of Φ. This result may be attributed the contaminant particles that have diffused into and subsequently sorbed onto the fracture matrix.

0.4.6 Co–Transport Effects

Variation of the co–transport parameter, K_n, affects the transport behavior of contaminants as shown in Figure 0.16. The leading breakthrough curve corresponds to the colloid plume, unaffected by the transport conditions to which the contaminants are subjected; the slowest curve corresponds to a contaminant plume that does undergo sorption onto the colloids ($K_n = 0.0$). It is evident that as the co–transport parameter is increased, more contaminants undergo sorption onto colloids, and the contaminant breakthrough curve approaches the colloid breakthrough curve.

Figure 0.17 illustrates a succession of snapshots in time showing the x– and y–locations of the individual components of a contaminant plume undergoing advection, diffusion, and co–transport processes. The contaminant particles that are sorbed onto colloid particles are clearly toward the front of the plume due to their adoption of the transport properties of the faster moving colloid plume. Contaminants that have not undergone sorption onto colloid particles make up the trailing part of the plume.

0.4.7 All Parameters

Figure 0.18 shows the effect on the contaminant breakthrough curves when matrix diffusion, wall sorption and co–transport processes are incorporated in the model. Three reference curves are included to aid in the comparison. The first curve shows the effect of co–transport only, resulting in complete breakthrough of the plume (due to the lack of wall sorption) and significantly earlier breakthrough times in relation
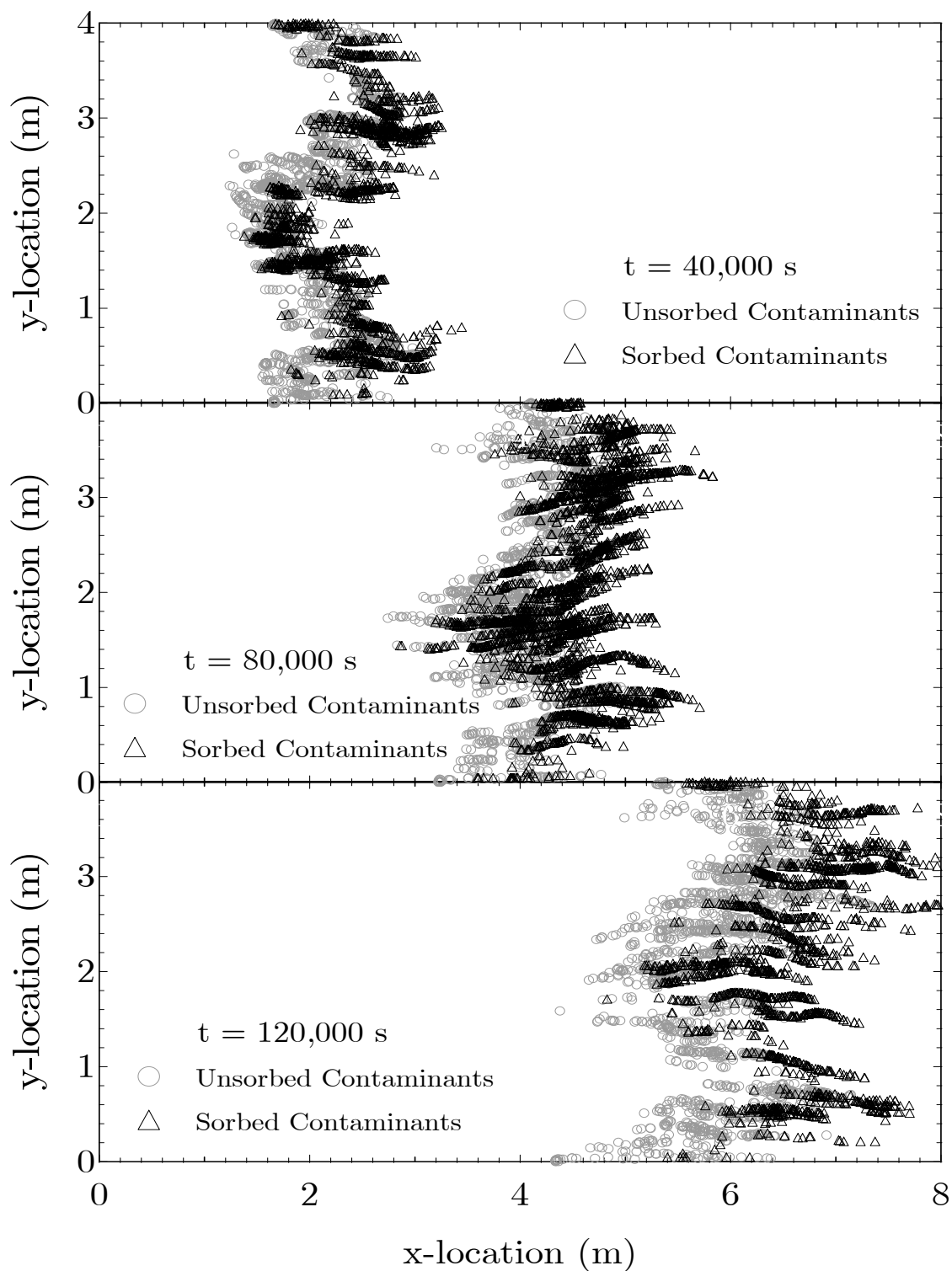
Figure 0.17: Snapshots in time of a contaminant plume traveling through a variable aperture fracture undergoing advection, diffusion, and co–transport.
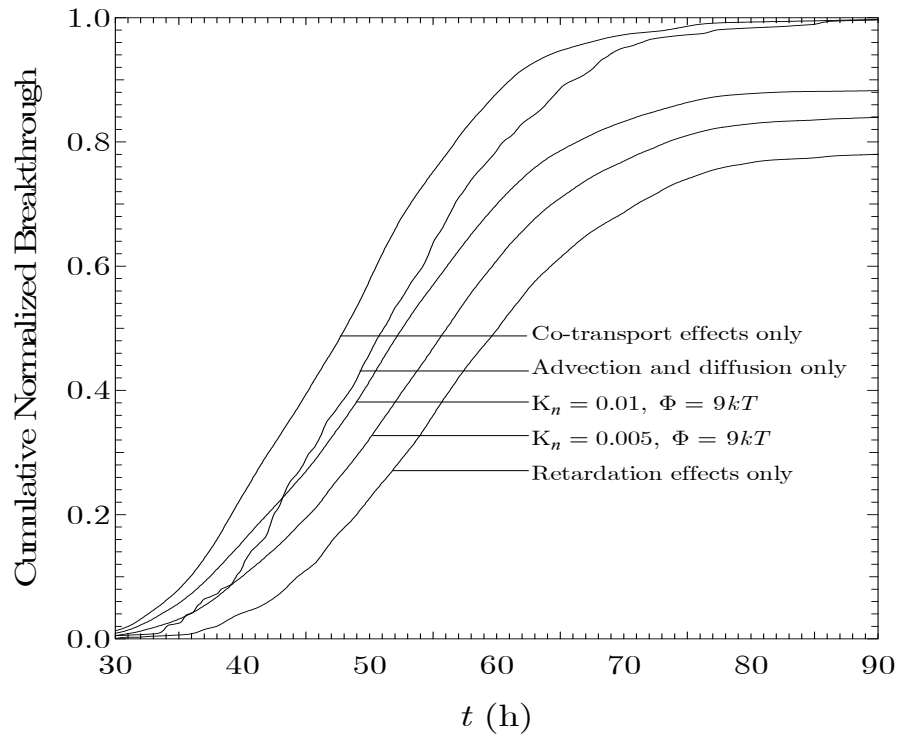
Figure 0.18: Contaminant breakthrough curves resulting from inclusion of matrix diffusion, wall sorption and co–transport processes.

to the other cases. The second curve shows the result of subjecting the plume only to advective and diffusive forces, and is considered the base or reference case. The last curve shows the effects of including only retardation forces (i.e., wall sorption and matrix diffusion) in the model. This curve indicates that a significant portion of the plume remains sorbed on the fracture walls or diffused within the surrounding medium.

When the model is run with all transport, retardation and reaction phenomena acting on the plumes, the effect on the breakthrough curves may be seen by looking at the normalized number of particles eluted. Rather than sorb onto the walls of the

fracture, many contaminant particles sorb preferentially onto colloid particles and continue moving through the fracture, resulting in increased elution.

0.5   Conclusion

A quasi–three–dimensional particle tracking model is used to investigate the effects of matrix diffusion, wall deposition, and co–transport on the transport properties of plumes of contaminants and colloids flowing through a variable aperture fracture subject to advective and diffusive mass transfer. Using breakthrough curves plotting the cumulative normalized number of particles eluted as a function of residence time, it is shown that matrix diffusion and wall sorption processes serve to retard the transport of a contaminant plume, while co–transport enhances contaminant mobility. Wall sorption was shown to decrease the number of colloids eluted from the fracture, however colloids were not subjected to matrix diffusion and their transport properties were unaffected by sorption phenomena with contaminants.

Linear correlations between the fifty percent elution time of a contaminant plume and the co–transport parameter were shown for the cases of co–transport both in the presence and absence of wall sorption and matrix diffusion processes.

Due to computational limitations, an instantaneous injection rather than constant concentration case is considered in this work. A constant concentration boundary condition merits further exploration, and will be studied as computational resources and technology decrease in cost. Further investigation of correlation between elution

time and co–transport parameters is merited to determine the functional relation-
ships among the relevant parameters. A polydisperse case should also be considered,
with the particle–particle sorption parameter defined as a function of particle diame-
ter. Reversible sorption cases, incorporation of gravititational forces and variation of
fracture characteristics may be investigated as well.

Bibliography

Abdel-Salam, A., Modeling of contaminant/colloid transport and unsaturated flow in fractured media, Ph.D. thesis, Univ. Calif. Irvine, 1995.

Abdel-Salam, A., and C. V. Chrysikopoulos, Analysis of a model for contaminant transport in fractured media in the presence of colloids, *J. Hydrol.*, *165*, 261–281, 1995a.

Abdel-Salam, A., and C. V. Chrysikopoulos, Modeling of colloid and colloid–facilitated contaminant transport in a two–dimensional fracture with spatially variable aperture, *Transp. Porous Media*, *20*, 197–221, 1995b.

Adamczyk, Z., B. Siwek, and M. Zembala, Kinetics of localized adsorption of particles on homogeneous surfaces, *J. Colloid and Interface Sci.*, *151*, 351–367, 1991.

Adamczyk, Z., B. Siwek, and M. Zembala, Reversible and irreversible adsorption of particles on homogeneous surfaces, *Colloids and Surfaces*, *62*, 119–130, 1992a.

Adamczyk, Z., B. Siwek, M. Zembala, and P. Weroński, Kinetics of localized adsorption of colloid particles, *Langmuir*, *8*, 2605–2610, 1992b.

Banks, J., J. S. C. II, and B. L. Nelson, *Discrete–event System Simulation*, 2 ed., Prentice Hall, 1996.

Chrysikopoulos, C. V., and A. Abdel-Salam, Modeling colloid transport and deposition in saturated fractures, *Colloids Surfaces A: Physicochem. Eng. Aspects*, *121*, 189–202, 1997.

Chrysikopoulos, C. V., and Y. Sim, One–dimensional virus transport in homogeneous porous media with time dependent distribution coefficient, *J. Hydrol.*, *185*, 199–219, 1996.

Drever, J. I., *The Chemistry of Weathering*, Reidel, Dordrecht, 1985.

Elimelech, M., J. Gregory, X. Jia, and R. Williams, *Particle Deposition & Aggregation: Measurement, Modeling and Simulation*, Butterworth-Heinemann, 1995.

Grindrod, P., The impact of colloids on the migration and dispersal of radionuclides within fractured rock, *J. Contam. Hydrol.*, *13*, 167–181, 1993.

Gutjahr, A. L., Fast Fourier Transform for Random Field Generation, *Project report for los alamos grant, contract 4-r58-2690r*, New Mexico Institute of Mining and Technology, Socorro, New Mexico, 1989.

Haber, S., and H. Brenner, Effect of entrained colloidal particles in enhancing the transport of adsorbable chemical contaminants, *J. Colloid and Interface Sci.*, *155*, 226–246, 1993.

Hoffman, J. D., *Numerical Methods for Engineers and Scientists*, McGraw–Hill, 1992.

Ibaraki, M., and E. A. Sudicky, Colloid–facilitated contaminant transport in discretely fractured porous media 1. Numerical formulation and sensitivity analysis, *Water Resour. Res.*, *31*, 2945–2960, 1995.

James, S. C., Polydisperse cooloid transport in fractured media, Ph.D. thesis, Univ. Calif. Irvine, 2001.

James, S. C., and C. V. Chrysikopoulos, Transport of polydisperse colloid suspensions in a single fracture, *Water Resour. Res.*, *35*, 707–718, 1999.

James, S. C., and C. V. Chrysikopoulos, Polydisperse colloid transport through a variable aperture fracture, *Water Resour. Res.*, *36*, 1457–1466, 2000.

James, S. C., and C. V. Chrysikopoulos, Effective velocity and effective dispersion coefficient for finitely sized particles flowing in a uniform fracture, *Water Resour. Res.*, *000*, 2001a.

James, S. C., and C. V. Chrysikopoulos, An efficient particle tracking equation with a specified spatial step for the solution of the diffusion equation, *Chem Eng. Sci.*, *000*, 2001b.

Johns, R. A., J. S. Steade, L. M. Costanier, and P. V. Roberts, Nondestructive measurements of fracture aperture in crystalline rock cores using X–ray computed tomography, *J. Geophys. Res.*, *98*, 1889–1900, 1993.

Johnson, R., S. Ning, and M. Elimelech, Colloid transport in geochemically heterogeneous porous media: Modeling and measurements, *Env. Sci. Technol.*, *30*, 3284–3293, 1996.

Keller, A. A., High resolution non–destructive measurement and characterization of fracture apertures, *Int. J. Rock Mech. Min. Sci.*, *35*, 1037–1050, 1998.

Kessler, J. H., and J. R. Hunt, Dissolved and colloidal transport in a partially clogged fracture, *Water Resour. Res.*, *30*, 1195–1206, 1994.

Liu, H. H., G. S. Bodvarsson, and L. Pan, Determination of particle transfer in random walk particle methods for fractured porous media, *Water Resour. Res.*, *36*, 707–713, 2000.

McCarthy, J. F., and C. Degueldre, *Environmental Particles*, chap. 2, Lewis, Boca Raton, Florida, 1993.

McCarthy, J. F., and J. M. Zachara, Subsurface transport of contaminants, *Env. Sci. and Technol.*, *23*, 1989.

McTigue, D. F., R. C. Gilver, and J. W. Nunziato, Rheological effects of nonuniform particle distributions in dilute suspensions, *J. Rheology*, *30*, 1053–1076, 1986.

Press, W. H., S. A. Teukolsky, W. T. Vetterling, and B. P. Flannery, *Numerical Recipes in FORTRAN*, Cambridge University Press, 1992.

Rajagopalan, R., and R. Q. Chu, Dynamics of adsorption of colloidal particles in packed beds, *J. Colloid Interface Sci.*, *86*, 299–317, 1981.

Reimus, P. W., The use of synthetic colloids in tracer transport experiments in saturated rock fracture, Ph.D. thesis, Los Alamos National Laboratory, 1995, lA–13004–T.

Reimus, P. W., B. A. Robinson, and R. J. Glass, Aperture characteristics, saturated fluid–flow, and tracer–transport calculations for a natural fracture, in *High–level radioactive waste management*, pp. 2009–2016, 1993.

Small, H., Hydrodynamic chromatography: A technique for size analysis of colloidal particles, *J. Colloid Interface Sci.*, *48*, 147–161, 1974.

Song, L., and M. Elimelech, Transient deposition of colloidal particles in heterogeneous porous media, *J. Colloid Interface Sci.*, *167*, 301–313, 1994.

Taylor, G. I., Dispersion of soluble matter in solvent flowing slowly through a tube, *Proc. R. Soc. London A*, *219*, 186–203, 1953.

Thompson, A. F. B., and L. W. Gelhar, Numerical simulation of solute transport in three-dimensional, randomly heterogeneous porous media, *Water Resour. Res.*, *26*, 2541–2562, 1990.

Welty, J. R., C. E. Wicks, and R. E. Wilson, *Fundamentals of Momentum, Heat, and Mass Transfer*, 3 ed., John Wiley and Sons, 1984.